

**STUDY OF SURFACE PLASMON RESONANCE  
SENSOR BY USING POWELL LENS**

**Jordan Hakim Hossea**



**A Thesis Submitted in Partial Fulfillment of the Requirements for the  
Degree of Master of Engineering in Electronic  
and Photonic Engineering  
Suranaree University of Technology  
Academic Year 2016**

# การศึกษาเซ็นเซอร์แบบคลื่นผิวพลาสมอนโดยการใช้เลนส์โฟเวลด์



นายจอร์แดน ฮาคิม โฮสเซีย

วิทยานิพนธ์นี้เป็นส่วนหนึ่งของการศึกษาตามหลักสูตรปริญญาวิศวกรรมศาสตรมหาบัณฑิต

สาขาวิชาวิศวกรรมอิเล็กทรอนิกส์และฟิสิกส์

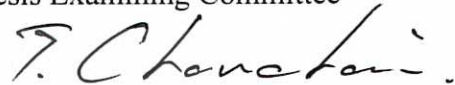
มหาวิทยาลัยเทคโนโลยีสุรนารี

ปีการศึกษา 2559

**STUDY OF SURFACE PLASMON RESONANCE SENSOR  
BY USING POWELL LENS**

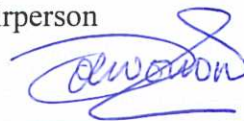
Suranaree University of Technology has approved this thesis submitted in partial fulfillment of the requirements for a Master's Degree.

Thesis Examining Committee



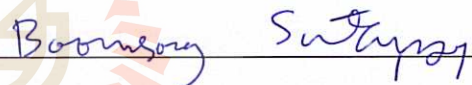
(Assoc. Prof. Dr. Chanchai Thongsopa)

Chairperson



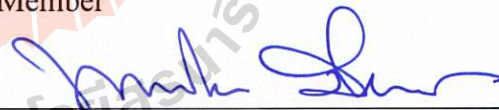
(Prof. Dr. Joewono Widjaja)

Member (Thesis Advisor)



(Asst. Prof. Dr. Boonsong Sutapun)

Member



(Asst. Prof. Dr. Panomsak Meemon)

Member



(Prof. Dr. Sukit Limpijumnong)

Vice Rector for Academic Affairs  
and Innovation



(Assoc. Prof. Flt. Lt. Dr. Kontorn Chamniprasart)

Dean of Institute of Engineering


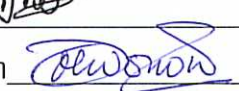
จอร์แดน ฮาคิม โฮสเซีย : การศึกษาเซ็นเซอร์แบบคลื่นผิวพลาสมอนโดยใช้เลนส์  
โพเวลล์ (STUDY OF SURFACE PLASMON SENSOR BY USING POWELL LENS)  
อาจารย์ที่ปรึกษา : ศาสตราจารย์ ดร.ยูวโน วิจิตยา, 46 หน้า

วิทยานิพนธ์ฉบับนี้เป็นการศึกษาการออกแบบเชิงแสงสำหรับเซ็นเซอร์แบบคลื่นผิวพลาสมอน โดยใช้เลนส์โพเวลล์ งานวิจัยนี้ได้ศึกษาผลกระทบของมุมเอียงและวัสดุของปริซึมต่อมุมของเลนส์โพเวลล์ ขนาดของลำแสงและขนาดของเซ็นเซอร์รับภาพ นอกจากนี้ยังศึกษาผลของตำแหน่งของลำแสงที่ตกกระทบปริซึม การยืนยันความเป็นไปได้ของการออกแบบเซ็นเซอร์ชนิดดังกล่าวจะเปรียบเทียบกับผลการทดลองการวัดค่าดัชนีหักเหของอากาศและน้ำ



มหาวิทยาลัยเทคโนโลยีสุรนารี

สาขาวิชาวิศวกรรมอิเล็กทรอนิกส์  
ปีการศึกษา 2559

ลายมือชื่อนักศึกษา   
ลายมือชื่ออาจารย์ที่ปรึกษา 

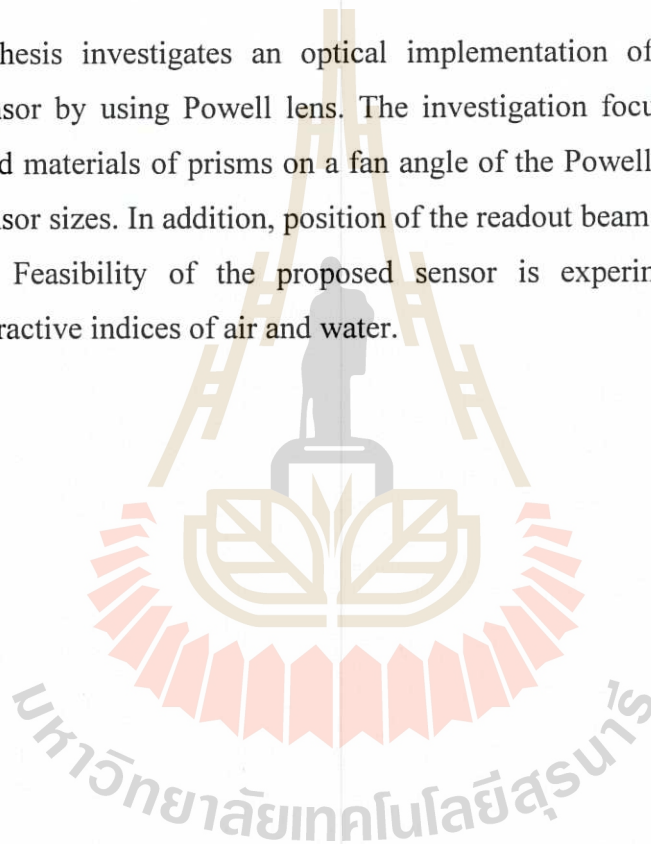
JORDAN HAKIM HOSSEA : STUDY OF SURAFCE PLASMON

RESONANCE SENSOR BY POWELL LENS. THESIS ADVISOR : PROF.

JOEWONO WIDJAJA, Ph.D., 46 PP.

SURFACE PLASMON RESONANCE / POWELL LENS

This thesis investigates an optical implementation of a surface plasmon resonance sensor by using Powell lens. The investigation focuses on effects of an apex angle and materials of prisms on a fan angle of the Powell lens, detected beam, and image sensor sizes. In addition, position of the readout beam impinges on prism is also studied. Feasibility of the proposed sensor is experimentally verified by measuring refractive indices of air and water.



School of Electronic Engineering

Academic Year 2016

Student's Signature \_\_\_\_\_

Advisor's Signature \_\_\_\_\_

## ACKNOWLEDGEMENTS

The author would like to thank Jesus for giving health and strength, enabling accomplishment of this thesis in the School of Electronic Engineering, Suranaree University of Technology Thailand.

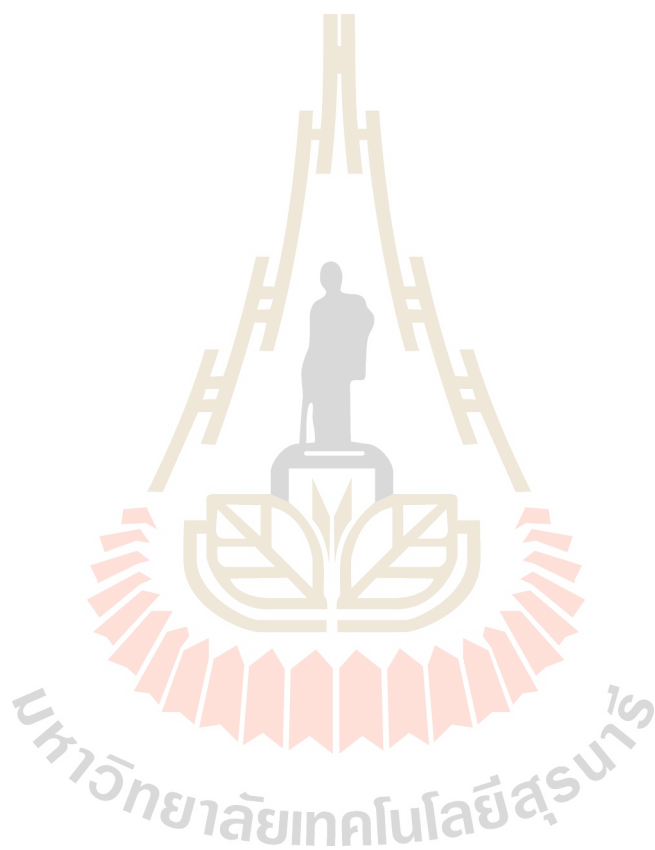
Many thanks should go to my thesis advisor, Prof. Dr. Joewono Widjaja for his guidance, encouragement, questions which stretches my thinking and financial support throughout my course of this study. I learned practically from him that commitment, persistence and discipline are required to achieve anything worthwhile. Also, special thanks should go to the committee, Assoc. Prof. Dr. Chanchai Thongsopa (Chairperson), Asst. Prof. Dr. Boonsong Sutapun (General Advisor), Asst. Prof. Dr. Panomsak Meemon (Member) for their advice, comment and encouragement.

Also, I would like to express my gratitude to Mr. Jirnavat Dantonglang (Mechanical laboratory technician in F1) who helped me to make prism and Powell lens holders. Again, it is my joy to express thanks to my friend Jaron Wongjarern for his support and willingness to share his idea on setting up optical experiments. More thanks should go to Mr. Taweesak Chaiyakhun for technical assistance.

In addition, I would like to express my grateful thanks to all graduates and staffs from the School of Electronic Engineering and School of Physics for their support and encouragement.

Finally, I would to thank my family including my beloved wife Flora J. Mangula and son Hospian for their encouragement, prayers and support.

Jordan Hakim Hossea



# TABLE OF CONTENTS

	<b>Page</b>
ABSTRACT (THAI) .....	I
ABSTRACT (ENGLISH).....	II
ACKNOWLEDGEMENTS .....	III
TABLE OF CONTENT .....	V
LIST OF TABLES .....	VII
LIST OF FIGURES .....	VIII
<b>CHAPTER</b>	
<b>I INTRODUCTION</b> .....	<b>1</b>
1.1 Surface Plasmon Resonance Sensor .....	1
1.2 Research Objectives .....	3
1.3 Scope and Limitation of the Study .....	4
1.4 Organization of the Thesis .....	5
<b>II THEORY</b> .....	<b>5</b>
2.1 General Theory of Surface Plasmon Resonance.....	6
2.2 Evanescent Wave .....	8
2.3 Surface Plasmon.....	10
2.3.1 Resonance by TM Wave .....	10
2.3.2 Resonance by TE Wave .....	13
2.4 Surface Plasmon Resonance .....	17



## TABLE OF CONTENTS (Continued)

	<b>Page</b>
2.5 Powell Lens.....	20
<b>III RESEARCH METHODOLOGY.....</b>	<b>22</b>
3.1 Proposed SPR Sensor.....	22
<b>IV EXPERIMENTAL VERIFICATIONS.....</b>	<b>32</b>
4.1 Experiments Setup.....	32
4.2 Measurement of the Fan Angle.....	33
4.3 Measurement of the Beam Size.....	35
4.4 Measurement of Refractive Index.....	36
<b>V CONCLUSION AND FUTURE WORK.....</b>	<b>40</b>
5.1 Conclusions.....	40
5.2 Future Work.....	41
<b>REFERENCES.....</b>	<b>42</b>
<b>BIOGRAPHY.....</b>	<b>46</b>

## LIST OF TABLES

Table	Page
3.1 Fan angles for different right angle prism materials.....	23
3.2 Fan angles for different equilateral prism materials .....	24
3.3 Beam sizes for different right angle prism materials.....	29
3.4 Beam sizes for different equilateral prism materials .....	30
4.1 Fan angles as a function of the CMOS sensor position .....	35
4.2 Beam sizes of SF 11 prism.....	35

## LIST OF FIGURES

Figure	Page
2.1 A schematic diagram of refraction and reflection of light with the incident angle $\beta_i$ at an interface of two media with refractive indices $n_1$ and $n_2$ .....	6
2.2 Schematic diagram of the TM-wave propagation at the interface between a metal and a dielectric.....	10
2.3 Schematic diagram of the TE-wave propagation at the interface between a metal and a dielectric.....	14
2.4 Variation of resonance angle with respect to changes in refractive index of the samples with different materials of the prism. ....	19
2.5 A schematic diagram of Powell lens .....	20
2.6 An intensity distribution of Powell lens. ....	21
3.1 A schematic diagram of a Kretschmann-based SPR sensor by using Powell lens .....	22
3.2 Dependence of $CH$ on $AJ$ for the prism side $AB = 5\text{cm}$ . ....	26
3.3 Dependence of $BG$ on $AJ$ for the prism side $AB = 5\text{cm}$ . ....	28
4.1 A schematic diagram of an optical setup for measuring the fan angle of the Powell lens .....	33
4.2 Diverging beam sizes measured at different positions $z$ .....	34
4.3 Intensity distribution of the reflected beam $GH$ at screen obtained without using the gold coated glass chip .....	36

**LIST OF FIGURES (Continued)**

<b>Figure</b>	<b>Page</b>
4.4 Intensity distribution of the reflected TE-mode beam GH.....	37
4.5 The intensity distribution of the reflected beam with two dip intensities caused by the resonances of air and water.....	38



# CHAPTER I

## INTRODUCTION

### 1.1 Surface Plasmon Resonance Sensor

Surface plasmons are electric charges, which oscillate at an interface between metal-dielectric medium. This surface plasmon can be excited with sources which are either electrons or photons (Raether, 1988). There are three optical methods to excite surface plasmon. These are prisms, waveguides, and grating couplers. Among these methods prism coupler is widely employed to transfer energy from photons to plasmons due to its simplicity. This is because direct illumination of metal – dielectric interface with light wave causes a mismatch between a wave vector of surface plasmon and that of the incident photons (Kretschmann and Raether, 1968). In order to equilibrate the two wave vectors, total internal reflection phenomenon in prism is employed. This prism coupling is accomplished by coating prism with a thin metal film. Read out beam is shone through the prism onto the metal film with dielectric sample is placed on top of the film. When the wave vector matching condition is reached, attenuated total internal reflection occurs at a certain angle, which is greater than a critical angle. At this state, photons energy is absorbed by free electrons in the metal surface, yielding surface plasmon resonance (SPR). As a result of the photon energy absorption, intensity of the reflected light reduces drastically. This resonance phenomenon can be used to monitor changes of the refractive index of a medium

adjacent to the metal layer by detecting shifts of light reflectance dip through an angular interrogation.

SPR sensor is the opto-electronic technique, which has captured many attentions in recent years. This is due to its numerous merits such as noninvasive, label free, real time, and needs very small amount of sample. Due to those features, SPR sensor has found applications in environmental monitoring such as detection of pollutants spilled on soil (Yap *et al*, 2011). Accurate and consistent detections of DNA in minimal quantity without label by using SPR sensor has been reported (Goodrich *et al*, 2004). Moreover, SPR sensor can be employed as a microscopic imaging system for observing culturing process of individual living cells such as mast cells, keratinocytes, basophils and B lymphocytes (Yanase *et al*, 2010; Laplatine *et al*, 2014). In food industry, SPR sensor has been applied in detection of bacteria and virus presence such as salmonella, toxoplasma, listeria in a very low level and fast rate (Koubova *et al*, 2001; Taylor *et al*, 2006; Bouguelia *et al*, 2013; Laplatine *et al*, 2014). SPR sensor also plays great role in detection of gases concentration (Tobiška *et al*, 2001), monitoring water quality and purity in urban and rural water supply system or in the environment surrounding toxic generating industries (Mouvet *et al*, 1997; Forzani *et al*, 2005). Apart from technical applications, it has been used to teach and motivate undergraduate students about physical chemistry and biology, because molecule interaction, antibody, antigen binding process and rate of chemical reaction can be observed and visualized (Lavine *et al*, 2007; Pluchery *et al*, 2011). In addition to those applications, energy absorption of SPR phenomenon has been proposed for bacterial sterilization (Dou *et al*, 2012).

The angular interrogation techniques can be implemented by using either mechanical scanning, converging, or diverging beam. In the mechanical scanning, the prism which is mounted on top of a turntable is rotated, while a photodetector is fixed to a position, which covers all ranges of the sample to be measured. The rotation mechanism can be done either manually or automatically through a stepper-motor. The demerits of this method make the set up to be bulky and costly. It is bulky because a distance between the light source and a photodetector should be large, in order to get higher angular resolution. This large separation causes mechanical noise and thermal drift (Tao *et al*, 2004). Therefore, in order to remove noises, optical filters and lenses are needed. Consequently, a lock - in amplifier is required to process signal output detected by sensitive photodetector (Yap *et al*, 2011). Additional optical components and instrumentations do not only increase the cost but also give hefty set up (Tao *et al*, 2004; Gwon and Lee, 2010; Pluchery *et al*, 2011; Mukhtar *et al*, 2013; Kashif *et al*, 2014).

The second method for matching of the wave vectors is by using a converging beam which circumvents the mechanical scanning problem (Schasfoort and McWhirter, 2008). This is done by collimating a read out beam and focusing it on a sensing area. A resultant reflected beam is collected by a photodetector through collimating lens. In this second method, the converging beam is regarded as a bundle of light rays travelling simultaneously with different angular directions. Irrespective of good resolution and sensitivity, the sensing area is small point. (Nikitin *et al*, 1999; Palumbo *et al*, 2003; Schermer, 2007)

Due to its simplicity, an implementation of a diverging beam-based SPR sensor by using a cylindrical lens has been reported (Chan and Jutamulia, 2012).

Although this method provides a compact setup without moving parts, however, the generated fan-shaped beam has a Gaussian intensity profile such as its intensity decreases gradually from maximum at the beam axis to minimum toward off-axis. As a consequence, it is hard to decide whether a detected minimum intensity is a result of either the plasmon resonance or the non-uniform Gaussian beam. Moreover, this lens has small divergence angle which results in small range of refractive index measurements and limited number of analyzable samples. However, laser line generator provides uniform intensity profile which makes easy to decide once the dip shift occurred.

## **1.2 Research Objectives**

- 1.2.1 To develop surface plasmon resonance sensor by using Powell lens.
- 1.2.2 To study effects of the position of the readout beam on the resonance angle detection.
- 1.2.3 To study effects of the apex angle and material of the prism on the fan angle and the read out beam size.
- 1.2.4 To determine the detector position with respect to the prism surface.

## **1.3 Scope of the Study**

- 1.3.1 The SPR sensor is developed by using the Kretschmann-based prism configuration.
- 1.3.2 Diverging beam is generated by Powell lens (Thorlabs, PL0160).
- 1.3.3 The experimental verifications measure the refractive indices of air and water.



## 1.4 Organization of the Thesis

The thesis is divided into five chapters. A general introduction, research objectives and scope of the study are given in the first chapter. Chapter 2 reviews theory of surface plasmon resonance and Powell lens. The proposed SPR sensor is discussed in Chapter 3. Experimental and analytical results are presented in Chapter 4. Chapter 5 summarizes the experimental measurements of refractive indices reached in this work.

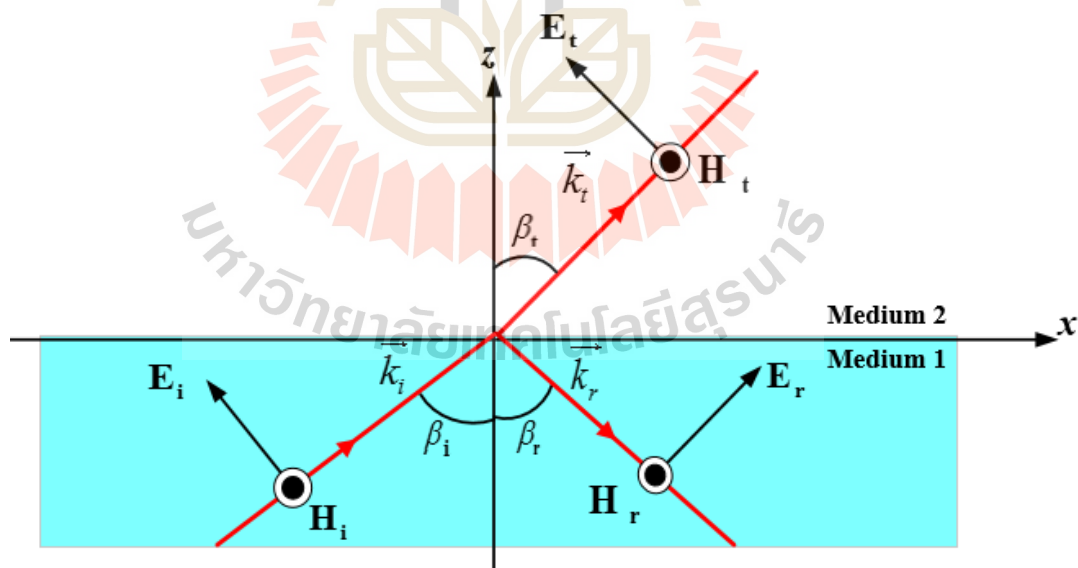


## CHAPTER II

### THEORY

#### 2.1 General Theory of Surface Plasmon Resonance

Surface plasmon resonance is an optical method for detecting or sensing changes in material properties such as refractive index. This method uses an evanescent wave for exciting surface plasmons in an interface between a thin metal layer and dielectric samples being analyzed. The evanescent wave is the electromagnetic wave which is generated when an incident angle of light inside a



**Figure 2.1** A schematic diagram of refraction and reflection of light with the incident angle  $\beta_i$  at an interface of two media with refractive indices  $n_1$  and  $n_2$ .

prism is greater than a critical angle. In order to excite surface plasmons, the evanescent wave needs to penetrate through the metal film. This can be accomplished because the normal component of the electric field vector is perpendicular to the interface of the metal-dielectric sample, while the tangential component propagates along the interface. This is true for the read out beam with a transverse magnetic (TM) polarization mode, where the electric field vector is parallel to the incident plane of the beam (Maier, 2007, Bordo and Rubahn, 2008).

Figure 2.1 shows the TM polarized wave incident at an oblique angle on an interface of two media with refractive indices  $n_1$  and  $n_2$ .  $\beta_i$ ,  $\beta_r$ , and  $\beta_t$  are the angles of the incidence, the reflected, and the transmitted waves, respectively.  $\vec{k}_i$ ,  $\vec{k}_r$  and  $\vec{k}_t$  correspond to the wave vectors of the incident, the reflected, and the transmitted wave propagations, respectively. From Fig 2.1, the wave vectors can be expressed into its components as

$$\begin{aligned}\vec{k}_i &= \vec{a}_x k_{ix} + \vec{a}_z k_{iz} = k_i \sin \beta_i \vec{a}_x + k_i \cos \beta_i \vec{a}_z \\ k_r &= \vec{a}_x k_{rx} - \vec{a}_z k_{rz} = k_r \sin \beta_r \vec{a}_x - k_r \cos \beta_r \vec{a}_z \\ k_t &= \vec{a}_x k_{tx} + \vec{a}_z k_{tz} = k_t \sin \beta_t \vec{a}_x + k_t \cos \beta_t \vec{a}_z,\end{aligned}\quad (2.1)$$

where  $\vec{a}_x$ ,  $\vec{a}_y$  and  $\vec{a}_z$  are the unit vectors in the directions of  $x$ ,  $y$ , and  $z$ , respectively.

The mathematical condition for the required TM wave to excite the surface plasmons can be explained as follows. The incident light wave is considered to have the electric field

$$\vec{E}_i(x, z) = E_{io} \left( -\vec{a}_x \cos \beta_i + \vec{a}_z \sin \beta_i \right) \exp[-jk_i(x \sin \beta_i + z \cos \beta_i)] \quad (2.2)$$

which is parallel to the incident plane that is the  $x$ - $z$  plane.  $E_{io}$  is the amplitude of the incident electric field. Consequently, the transmitted electric field can be written as

$$\vec{E}_t(x, z) = E_{io} \left( -\vec{a}_x \cos \beta_t + \vec{a}_z \sin \beta_t \right) \exp[-jk_t(x \sin \beta_t + z \cos \beta_t)] \quad (2.3)$$

Its incident magnetic field which is perpendicular to the electric field is given by

$$\vec{H}_i(x, z) = \frac{\vec{a}_y E_{io}}{\eta_1} \exp[-jk_i(x \sin \beta_i + z \cos \beta_i)], \quad (2.4)$$

while, the transmitted magnetic field is

$$\vec{H}_t(x, z) = \frac{\vec{a}_y E_{to}}{\eta_2} \exp[-jk_t(x \sin \beta_t + z \cos \beta_t)]. \quad (2.5)$$

Here,  $\eta_1$  and  $\eta_2$  are the intrinsic impedances of the media 1 and 2, respectively. The amplitude of the transmitted electric field  $E_{to}$  is equal to  $\tau E_{io}$  with  $\tau$  is the transmission coefficient.

## 2.2 Evanescent Wave

The evanescent field can be derived by considering the transmitted electric field, which is related to the incident field through Snell's law

$$n_1 \sin \beta_i = n_2 \sin \beta_t. \quad (2.6)$$

If the refractive index of the medium 1 is greater than that of the medium 2, the transmittance angle will be greater than the incident angle. As the incident angle increases to be equal to critical angle  $\beta_c$ , the transmittance angle becomes  $90^\circ$ . Thus Eq. (2.6) reduces to  $\sin \beta_c = n_2/n_1$ . This results in the propagation of the transmitted wave along the interface surface. When the incident angle is greater than the critical angle, the right-hand side of Eq. (2.7).

$$\sin \beta_t = \frac{n_1}{n_2} \sin \beta_i \quad (2.7)$$

becomes greater than unity. This will not give solution with real value for  $\beta_t$ , because

$$\cos \beta_t = \pm j \sqrt{\left(\frac{n_1}{n_2} \sin \beta_i\right)^2 - 1} \quad (2.8)$$

is imaginary. Substitution of Eq. (2.8) into Eq. (2.4) gives

$$\vec{E}_t(x, z) = \left(-E_x \vec{a}_x + E_z \vec{a}_z\right) \exp\left[-jk_t x \frac{n_1}{n_2} \sin \beta_i\right] \exp\left[\pm k_t z \sqrt{\left(\frac{n_1}{n_2} \sin \beta_i\right)^2 - 1}\right], \quad (2.9)$$

where  $E_x = E_{t0} \cos \beta_i$  and  $E_z = E_{t0} \sin \beta_i$ . For the sake of simplicity, Eq. (2.9) can be rewritten as

$$\vec{E}_t(x, z) = \left(-E_x \vec{a}_x + E_z \vec{a}_z\right) \exp[-jk_x x] \exp[-\kappa z], \quad (2.10)$$

with

$$\kappa = k_t \sqrt{\left(\frac{n_1}{n_2} \sin \beta_i\right)^2 - 1} \quad (2.11)$$

and

$$k_x = k_t \frac{n_1}{n_2} \sin \beta_i. \quad (2.12)$$

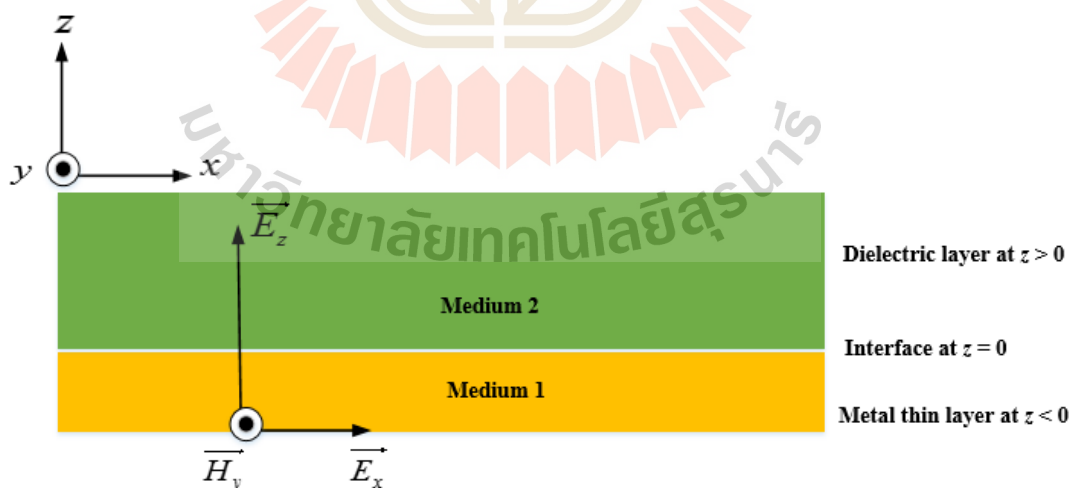
The second exponential term with negative sign is chosen because it is impossible to have an increasing field as distance  $z$  increases. Equation (2.10) is the mathematical expression of the evanescent wave, which will be used to derive the equation of the surface plasmon wave vector.

## 2.3 Surface Plasmon

Surface plasmons are free charge oscillations that occur at an interface between metal and a dielectric medium having frequency dependent dielectric constants.

### 2.3.1 Plasmon Resonance by TM Wave

In order to generate the surface plasmon resonance by the incident electromagnetic wave with the TM polarization, momentum of photons and plasmons need to match. This can be achieved by using the evanescent wave discussed in the previous section. Let us consider that evanescent wave propagates through planar media, i.e metal and dielectrics placed above the prism shown in Fig. 2.2. In this thesis,  $\epsilon_n$  and  $\mu_n$  are permittivity and permeability of the  $n^{\text{th}}$  medium.



**Figure 2.2** Schematic diagram of the TM-wave propagation at the interface

between a metal and a dielectric.

When the interface between the two media is located at  $z = 0$ , the electric field of the evanescent wave at the interface of the two media can be written as

$$\vec{E}_{t2}(x, z) = (-E_{x2}\vec{a}_x + E_{z2}\vec{a}_z)\exp[-jk_x x]\exp[-\kappa_2 z] \quad \text{for } z > 0 \quad (2.13)$$

and

$$\vec{E}_{t1}(x, z) = (-E_{x1}\vec{a}_x + E_{z1}\vec{a}_z)\exp[-jk_x x]\exp[\kappa_1 z] \quad \text{for } z < 0, \quad (2.14)$$

respectively. The propagation of the evanescent wave through the medium 1 can be expressed by using the wave equation

$$\frac{\partial^2 \vec{E}_{t1}(x, z)}{\partial x^2} + \frac{\partial^2 \vec{E}_{t1}(x, z)}{\partial y^2} + \frac{\partial^2 \vec{E}_{t1}(x, z)}{\partial z^2} = \mu_1 \varepsilon_1 \frac{\partial^2 \vec{E}_{t1}(x, z)}{\partial t^2}. \quad (2.15)$$

The second order derivation gives

$$-k_x^2 \vec{E}_{t1}(x, z) + (\kappa_1)^2 \vec{E}_{t1}(x, z) = -\omega^2 \mu_1 \varepsilon_1 \vec{E}_{t1}(x, z). \quad (2.16)$$

Dividing both side of Eq. (2.16) by  $\vec{E}_{t1}(x, z)$  gives

$$-k_x^2 + \kappa_1^2 = -\omega^2 \mu_1 \varepsilon_1 \quad (2.17)$$

or

$$\kappa_1^2 = k_x^2 - \omega^2 \mu_1 \varepsilon_1. \quad (2.18)$$

In the medium 2, the evanescent wave propagation follows

$$\frac{\partial^2 \vec{E}_{t2}(x, z)}{\partial x^2} + \frac{\partial^2 \vec{E}_{t2}(x, z)}{\partial y^2} + \frac{\partial^2 \vec{E}_{t2}(x, z)}{\partial z^2} = \mu_2 \varepsilon_2 \frac{\partial^2 \vec{E}_{t2}(x, z)}{\partial t^2} \quad (2.19)$$

or

$$-k_x^2 \vec{E}_{t2}(x, z) + (-\kappa_2)^2 \vec{E}_{t2}(x, z) = -\omega^2 \mu_2 \varepsilon_2 \vec{E}_{t2}(x, z), \quad (2.20)$$

which can be written as

$$\kappa_2^2 = k_x^2 - \omega^2 \mu_2 \varepsilon_2. \quad (2.21)$$

The expression of the magnetic field of the evanescent wave can be derived from the following relationship (Maier, 2007)

$$\frac{\partial \vec{H}(x, z)}{\partial z} = -\varepsilon \frac{\partial \vec{E}(x, z)}{\partial t}. \quad (2.22)$$

For the medium 1, substitution of Eq. (2.13) into Eq. (2.22) gives

$$\frac{\partial \vec{H}_{t1}(x, z)}{\partial z} = -\varepsilon_1 \frac{\partial \vec{E}_{t1}(x, z)}{\partial t} \quad (2.23)$$

or

$$\vec{H}_{t1}(x, z) = -\varepsilon_1 \int \frac{\partial \vec{E}_{t1}(x, z)}{\partial t} dz. \quad (2.24)$$

Solving this equation gives the magnetic field as

$$\vec{H}_{t1}(x, z) = \frac{-j\omega\varepsilon_1 \vec{E}_{t1}(x, z)}{-\kappa_1}. \quad (2.25)$$

The magnetic and the electric fields in the medium 2 are related by

$$\frac{\partial \vec{H}_{t2}(x, z)}{\partial z} = -\varepsilon_2 \frac{\partial \vec{E}_{t2}(x, z)}{\partial t}. \quad (2.26)$$

In similar fashion, the magnetic field is found to be

$$\vec{H}_{t2}(x, z) = \frac{-j\omega\varepsilon_2 \vec{E}_{t2}(x, z)}{\kappa_2}. \quad (2.27)$$

According to the boundary condition of the interface problem, the tangential components of the two fields are continuous. Therefore,

$$\vec{H}_{t1} = \vec{H}_{t2} \quad (2.28a)$$

and

$$\vec{E}_{t1} = \vec{E}_{t2}. \quad (2.28b)$$

Consequently, the magnetic fields in the two media are related as



$$\frac{-j\omega\varepsilon_1\vec{E}_{t1}(x,z)}{-\kappa_1} = \frac{-j\omega\varepsilon_2\vec{E}_{t2}(x,z)}{\kappa_2} \quad (2.29)$$

Since  $\vec{E}_{t1} = \vec{E}_{t2}$ , the relationship between the wave vectors perpendicular to the interface in the two media can be obtained from Eq. (2.29) as

$$\frac{\varepsilon_1}{\kappa_1} = \frac{-\varepsilon_2}{\kappa_2} \quad (2.30)$$

or

$$\kappa_1 = -\frac{\varepsilon_1\kappa_2}{\varepsilon_2} = -\frac{\varepsilon_0\varepsilon_{r1}\kappa_2}{\varepsilon_0\varepsilon_{r2}} = -\frac{\varepsilon_{r1}\kappa_2}{\varepsilon_{r2}}. \quad (2.31)$$

Negative sign means that surface plasmon wave exists only at interface between the materials with opposite signs of the relative permittivities. Substitution of Eq. (2.31) into Eq. (2.18) results in

$$\left(-\frac{\varepsilon_{r1}\kappa_2}{\varepsilon_{r2}}\right)^2 = (k_x)^2 - \omega^2\mu_1\varepsilon_1. \quad (2.32)$$

Further derivation of Eq. (2.32) gives the wave vector of the surface plasmon

$$k_x = \frac{\omega}{c} \sqrt{\frac{\varepsilon_{r1}\varepsilon_{r2}}{\varepsilon_{r1} + \varepsilon_{r2}}}. \quad (2.33)$$

Here,  $\varepsilon_{r1}$  is the relative permittivity of the thin metallic medium 1 such as gold layer.

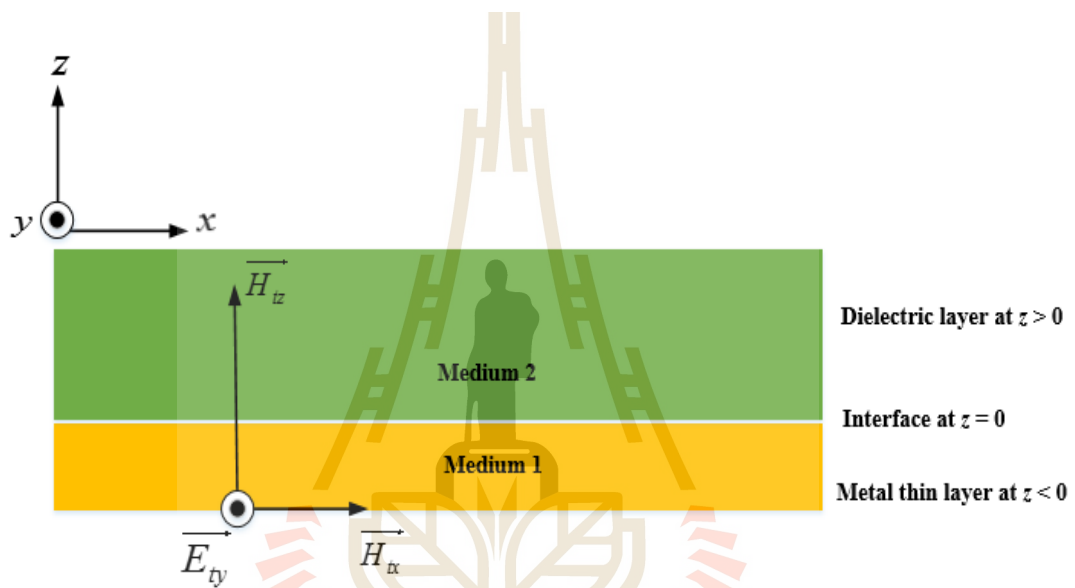
While  $\varepsilon_{r2}$  is the relative permittivity of the medium 2, which is the dielectric sample to be analyzed. Equation (2.33) is also known as the dispersion equation.

### 2.3.2 Plasmon Resonance by TE Wave

In order to generate surface plasmon by using the evanescent wave with the TE polarization, the required media need to be magnetic materials with

opposite polarities. This concept can be mathematically explained by using following discussion.

In order to derive the occurrence of the surface plasmon resonance by the TE wave, let us consider the propagation evanescent wave through the planar media placed above the prism shown in Fig. 2.3. The electric field of the



**Figure 2.3** Schematic diagram of the TE-wave propagation at the interface between a metal and a dielectric.

evanescent wave at the interface of the two media located at  $z = 0$  can be written as

$$E_{ty2}(x, z) = (E_{0y2} \vec{a}_y) \exp[-jk_x x] \exp[-\kappa_2 z] \quad \text{for } z > 0, \quad (2.35)$$

and

$$E_{ty1}(x, z) = (E_{0y1} \vec{a}_y) \exp[-jk_x x] \exp[\kappa_1 z] \quad \text{for } z < 0 \quad (2.34)$$

respectively. In the medium 1, the propagation of the evanescent wave follows

$$-k_x^2 \overrightarrow{E}_{ty1}(x, z) + (-\kappa_1)^2 \overrightarrow{E}_{ty1}(x, z) = -\omega^2 \mu_1 \varepsilon_1 \overrightarrow{E}_{ty1}(x, z). \quad (2.36)$$

Equation (3.36) can be written as

$$-k_x^2 + \kappa_1^2 = -\omega^2 \mu_1 \varepsilon_1 \quad (2.37)$$

or

$$\kappa_1^2 = k_x^2 - \omega^2 \mu_1 \varepsilon_1. \quad (2.38)$$

In the medium 2, the evanescent wave propagation results in

$$\kappa_2^2 = k_x^2 - \omega^2 \mu_2 \varepsilon_2. \quad (2.39)$$

According to Maier (Maier, 2007), the magnetic field of the evanescent wave can be derived from this general relationship

$$H_{tx}(x, z) = -\frac{1}{\mu_r \mu_o} \int \frac{\partial E_{ty}(x, z)}{\partial z} \partial t, \quad (2.40)$$

which results in

$$H_{tx}(x, z) = \frac{-\kappa}{j\omega \mu_r \mu_o} E_{ty}(x, z). \quad (2.41)$$

For the medium 1, Eq. (2.41) is equal to

$$H_{tx1}(x, z) = \frac{-\kappa_1}{j\omega \mu_{r1} \mu_o} E_{ty1}(x, z) \quad (2.42)$$

The magnetic and the electric fields in the medium 2 are related by

$$H_{tx2}(x, z) = -\frac{1}{\mu_{r2} \mu_o} \int \frac{\partial E_{ty2}(x, z)}{\partial z} \partial t. \quad (2.43)$$

The solution of Eq. (2.43) becomes

$$H_{tx2}(x, z) = \frac{-\kappa}{j\omega \mu_r \mu_o} E_{ty2}(x, z). \quad (2.44)$$

Therefore, the magnetic field in medium 2 is found to be

$$H_{tx2}(x, z) = \frac{\kappa_2}{j\omega\mu_{r2}\mu_o} E_{ty2}(x, z). \quad (2.45)$$

Since the tangential components of the two fields are continuous, therefore,

$$\overrightarrow{H}_{tx1}(x, z) = \overrightarrow{H}_{tx2}(x, z) \quad (2.46)$$

and

$$\overrightarrow{E}_{ty1}(x, z) = \overrightarrow{E}_{ty2}(x, z). \quad (2.47)$$

Consequently, the magnetic fields in the two media are related as

$$\frac{-\kappa_1}{j\omega\mu_{r1}\mu_o} E_{ty1}(x, z) = \frac{\kappa_2}{j\omega\mu_{r2}\mu_o} E_{ty2}(x, z) \quad (2.48)$$

Since  $\overrightarrow{E}_{ty1}(x, z) = \overrightarrow{E}_{ty2}(x, z)$ , the relationship between the wave vectors perpendicular to the interface between the two media can be obtained from Eq. (2.48) as

$$\frac{\kappa_1}{\mu_{r1}} = \frac{-\kappa_2}{\mu_{r2}} \quad (2.49)$$

or

$$\kappa_1 = \frac{-\mu_{r1}\kappa_2}{\mu_{r2}}. \quad (2.50)$$

Unlike Eq. (2.31), the negative sign now means that surface plasmon wave can be produced only at the interface between the materials with opposite sign of the relative permeabilities. Furthermore, substitution of Eq. (2.50) into Eq. (2.39) results in

$$\left( \frac{-\mu_{r1}\kappa_2}{\mu_{r2}} \right)^2 = (k_x)^2 - \omega^2 \mu_1 \epsilon_1. \quad (2.51)$$

By substituting Eq. (2.39) into Eq. (2.51), the wave vector of the surface plasmon can be obtained as

$$k_x = \frac{\omega}{c} \sqrt{\left[ \frac{\mu_{r1}\mu_{r2}(\epsilon_{r1}\mu_{r2} - \epsilon_{r2}\mu_{r1})}{(\mu_{r2} - \mu_{r1})(\mu_{r2} + \mu_{r1})} \right]}, \quad (2.52)$$

where  $\mu_{r1}$  and  $\mu_{r2}$  are the relative permeabilities of the media 1 and 2, respectively. Equation (2.52) shows that the required condition for the generation of the surface plasmon is to use the magnetic materials with different polarity. Since no natural material with this property has been found, thus it is difficult to generate the surface plasmon resonance with the TE wave.

## 2.4 Surface Plasmon Resonance

In the preceding sections, the required conditions for generating the surface plasmons by using the TM and TE waves have been discussed. It is found that the plasmon generation is applicable to the TM-wave-based configuration. In this section, a resonance condition of the surface plasmon is analyzed.

When the light beam is incidence at an appropriate angle called the resonance angle, photons and surface plasmon have the same momentum. Therefore, the surface plasmon resonance occurs. Due to the boundary condition, the tangential component of the wave vector of the incident electric field is the same as that of the tangential wave-vector of the transmitted electric field

$$k_x = k_i \sin \beta_i = k_t \sin \beta_t. \quad (2.53)$$

Since the wave vector of the incident electric field is originated from the prism, it can be expressed as

$$k_i = n_p \omega c = \frac{n_p 2\pi}{\lambda}, \quad (2.54)$$

with  $n_p$  is the refractive index of the prism. Therefore, the tangential component of the wave vector can be written as

$$k_x = \frac{2\pi n_p}{\lambda} \sin \beta_i. \quad (2.55)$$

According to Otto (Otto, 1968), the magnitude of the photon momentum of the evanescent wave is defined as

$$p_{eva} = \hbar k_x. \quad (2.56)$$

Substitution of Eq. (2.55) into Eq. (2.56) gives

$$p_{eva} = \frac{n_p h}{\lambda} \sin \beta_i. \quad (2.57)$$

In the case of the surface plasmon, its momentum magnitude can be determined by using Eq. (2.33)

$$p_{sp} = \frac{h}{\lambda} \sqrt{\frac{\epsilon_{r1} \epsilon_{r2}}{\epsilon_{r1} + \epsilon_{r2}}}. \quad (2.58)$$

In order to achieve the resonance condition, the momentum of the surface plasmon must be equal to the momentum of the evanescent wave

$$p_{eva} = p_{sp}. \quad (2.59)$$

Equating Eq. (2.58) and Eq. (2.59) yields

$$\frac{n_p h}{\lambda} \sin \beta_i = \frac{h}{\lambda} \sqrt{\frac{\epsilon_{r1} \epsilon_{r2}}{\epsilon_{r1} + \epsilon_{r2}}} \quad (2.60)$$

or

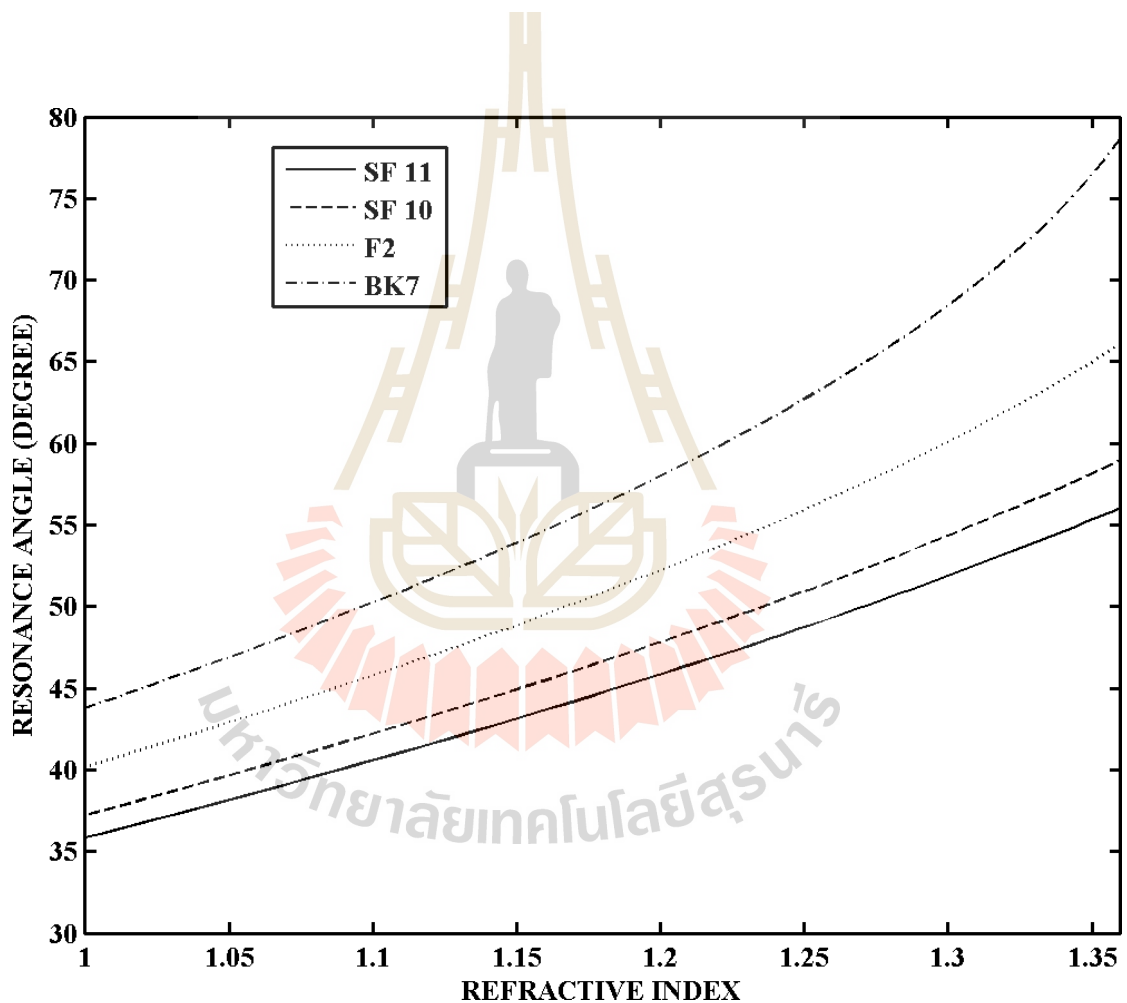
$$\beta_{spr} = \sin^{-1} \left( \frac{1}{n_p} \sqrt{\frac{\epsilon_{r1} \epsilon_{r2}}{\epsilon_{r1} + \epsilon_{r2}}} \right), \quad (2.61)$$

where  $\beta_{spr}$  stands for the incident angle  $\beta_i$  which causes the resonance occurrence.

Equation (2.61) reveals that the resonance angle depends on the refractive index of the prism material, the dielectric constants of the metal and the sample to be measured.

Therefore, this equation plays an important role in selection of the prism material for testing dielectric samples.

Figure 2.4 has been plotted by using Eq. (2.61). From the Fig. 2.4 shows that the prism with higher refractive index has almost linear relationship between resonance angle and refractive index of the sample for example SF11(1.785). While prism with low refractive index has nonlinear property for example BK7 (1.51).



**Figure 2.4** Variation of resonance angle with respect to changes in refractive index of the samples in different material of the prism.

## 2.5 Powell Lens

Powell lens was invented by Ian Powell in 1986. It is an optical lens which is used to convert Gaussian beam into uniform beam line. Normally, laser beam intensity exits from a laser head appears to be brighter at the center than at its other ends. This may limit its applications where uniform intensity light distribution required. Figure 2.5 shows a schematic diagram of Powell lens which has two surfaces namely the primary and the secondary surfaces. The primary surface has an

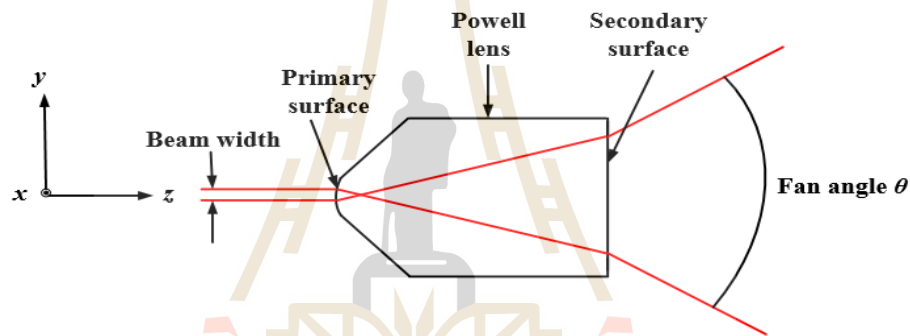


Figure 2.5 A schematic diagram of Powell lens.

apex and is responsible for spreading out light radiation more rapidly at its center than edges. The secondary surface is to increase the divergence of the incidence fan rays by using the principles of refraction. The primary surface has surface profile defined in the Cartesian coordinates system as

$$z = \frac{cy^2}{1 + (1 - (1 + Q)c^2y^2)^{1/2}}, \quad (2.65)$$



where  $y$  and  $z$  are independent of  $x$ ,  $c$  is the curvature at the apex and  $Q$  is the conic constant. The magnitude of the product  $Q.c$  lies between  $0.25$  and  $50\text{mm}^{-1}$  and  $Q$  is less than  $-1$ .

Figure 2.6 illustrates an example of a light intensity distribution generated by the Powell lens. The intensity distribution at the center is almost uniform, while at those their extremities fluctuated and becomes higher. This might be caused by a beam diameter which has bigger size than the apex of the primary surface.

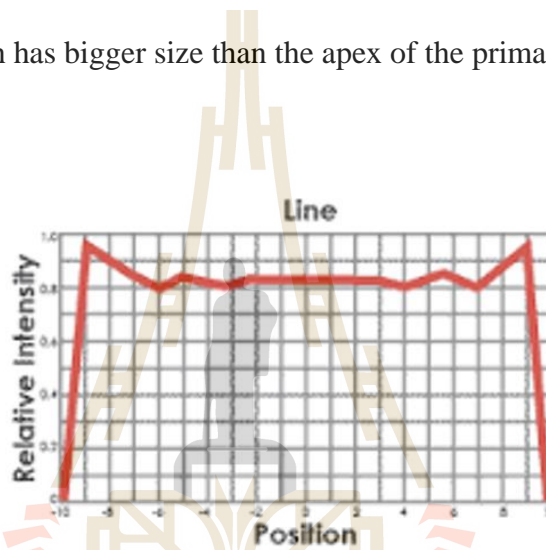
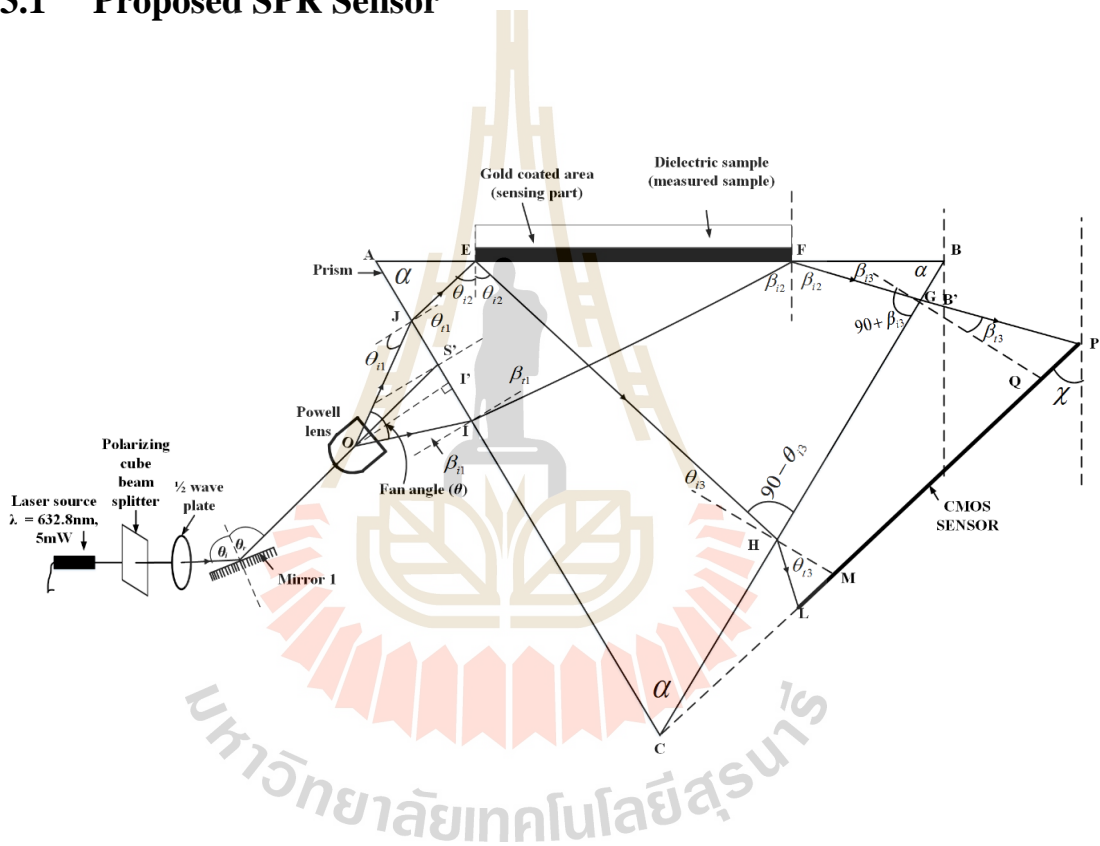


Figure 2.6 An intensity distribution of Powell lens.

# CHAPTER III

## RESEARCH METHODOLOGY

### 3.1 Proposed SPR Sensor



**Figure 3.1** A schematic diagram of a Kretschmann-based SPR sensor by using Powell lens.

Figure 3.1 shows a schematic diagram of an optical set up for implementing Kretschmann-based SPR sensor by using Powell lens. A glass plate with evaporated gold film having a refractive index of  $0.1728+j3.4218$  (Yamamoto, 2002; Mukhtar, Menon *et al.* 2013) is placed on top of the equilateral prism. In order to diminish loss

of the light refracted from the prism, the gap between the glass plate and the prism is filled with immersion oil. To perform measurements, sample solution is placed on the gold layer. Readout beam with the TM polarization is generated by passing laser light with a wavelength  $\lambda=632.8\text{nm}$  through a polarizing beam splitter and a half-wave plate. After being reflected by a mirror 1, the TM beam is diverged by using Powell lens into the line beam. The effects of the prism on the detected beam is studied by using three refractive indices of 1.785 (SF11), 1.728 (SF10) and 1.62 (F2). The proposed sensor is designed by considering that the diverging beam incident on the interface has a fan angle correspond to analyzable range of refractive indices. Thus, the ray  $JE$  is set to impinge at the critical angle of the prism  $\theta_{i2} = \theta_c$ , while the ray  $IF$  must have an incident angle which is greater than the resonance angle of the highest refractive index to be measured. When the angle of the ray  $JE$  is determined, the corresponding incident angles  $\theta_{i1}$  and  $\theta_{i3}$  at the surfaces  $AC$  and  $BC$  can be calculated.

The angles  $\beta_{i1}$  and  $\beta_{i3}$  can also be obtained by using  $\beta_{i2}$  maximum. Next, the fan angle of the readout beam is calculated as the summation of the incident angles  $\theta_{i1}$  and  $\beta_{i1}$

$$\theta = \theta_{i1} + \beta_{i1}. \quad (3.1)$$

**Table 3.1** Fan angles for different right angle prism material.

Prism RI	$\beta_{spr}$ (°)	$\theta_{i2}$ (°)	$\beta_{i2max}$ (°)	$\theta_{i1}$ (°)	$\beta_{i1}$ (°)	$\theta$ (°)
<b>1.785</b>	54.07	34.07	65	19.78	37.67	57.4
<b>1.728</b>	56.7	35.35	65	16.82	36.22	53.05
<b>1.620</b>	63.13	38.19	65	11.19	33.64	44.83

Table 3.1 shows the critical, the resonance and the required fan angles for the measurements of water with refractive index 1.331 (Fan and Longtin 2000) by using the right angle prism. The critical and the resonance angles are calculated by using Eqs. (2.6) and (2.61), respectively. Their values are used to determine the incident angles  $\theta_{i1}$  and  $\beta_{i1}$ . The fan angle is calculated by using Eq. (3.1). The result show that the prism with lower refractive index requires smaller fan angle.

Table 3.2 shows the calculated angles for the case of the equilateral prisms. The same dependency of the fan angles on the prism material is found. Thus, the fan angle does not only depend on the resonance angle, but also on the refractive index and the apex angle of the prism.

**Table 3.2** Fan angles for different equilateral prism materials.

Prism RI	$\beta_{spr}$ (°)	$\theta_{i2}$ (°)	$\beta_{i2max}$ (°)	$\theta_{i1}$ (°)	$\beta_{i1}$ (°)	$\theta$ (°)
<b>1.785</b>	54.07	34.07	65	51.3	8.95	60.26
<b>1.728</b>	56.7	35.35	65	46.09	8.662	54.57
<b>1.620</b>	63.13	38.19	65	37.14	8.117	45.26

The beams sizes  $IJ$ ,  $EF$  and  $HG$  that are incident on three sides of the prism can be calculated by using geometries of light propagations. From three triangles  $\Delta OIJ$ ,  $\Delta OI'J$  and  $\Delta OII'$ , the beam size  $IJ$  is related to the fan angle according to

$$IJ = \frac{OI' \sin \theta}{\cos \beta_{i1} \cos \theta_{i1}}, \quad (3.2)$$

where  $OI'$  is the distance from the Powell lens to the prism surface  $AC$ .

Before the beam sizes on  $EF$  and  $GH$  are derived, there is a need of establishing criteria for choosing the value of the distance  $AJ$ . The dependency of the ray  $EH$  upon  $AJ$  can be analyzed by considering the polygon  $EJHC$ . The length  $CH$  is related to  $AJ$  through this expression

$$CH = \frac{(AB - AJ) \sin \left( 2\theta_{i_2} - \tan^{-1} \left( \frac{CJ \cos(\alpha - \theta_{i_2}) \cos \theta_{i_2}}{AJ \sin \alpha + CJ \sin(\alpha - \theta_{i_2}) \cos \theta_{i_2}} \right) \right)}{\sin \left\{ \tan^{-1} \left( \frac{CJ \cos(\alpha - \theta_{i_2}) \cos \theta_{i_2}}{AJ \sin \alpha + CJ \sin(\alpha - \theta_{i_2}) \cos \theta_{i_2}} \right) \right\}}. \quad (3.3)$$

Equation (3.3) is a general condition for the ray  $EH$  to strike at a correct position on the prism side  $BC$  for both the equilateral and right angled prisms. However, the value of  $CJ$  differs for both prisms. For the equilateral prism which has equal side length  $AB=AC=BC$ ,

$$CJ = AC - AJ = AB - AJ, \quad (3.4a)$$

while for the right-angled prism

$$CJ = AC - AJ = AB \frac{\sqrt{2}}{2} - AJ. \quad (3.4b)$$

The distance  $CH$  can become zero due to the increase of  $AJ$ . In this case, the ray  $EH$  which is incident on the vertex  $C$  will be refracted into the ray  $HL$ .

The effect of the  $AJ$  on the position of the beam  $EF$  can be mathematically obtained by considering triangles  $\triangle AEJ$  and  $\triangle AFI$ . The derivation results are

$$AE = \frac{AJ \cos(\theta - \theta_{i_2})}{\cos \theta_{i_2}} \quad (3.5)$$

and

$$BF = \frac{AB \cos \beta_{i_2} - (AJ + IJ) \cos(\beta_{i_2} - \alpha)}{\cos \beta_{i_2}}. \quad (3.6)$$

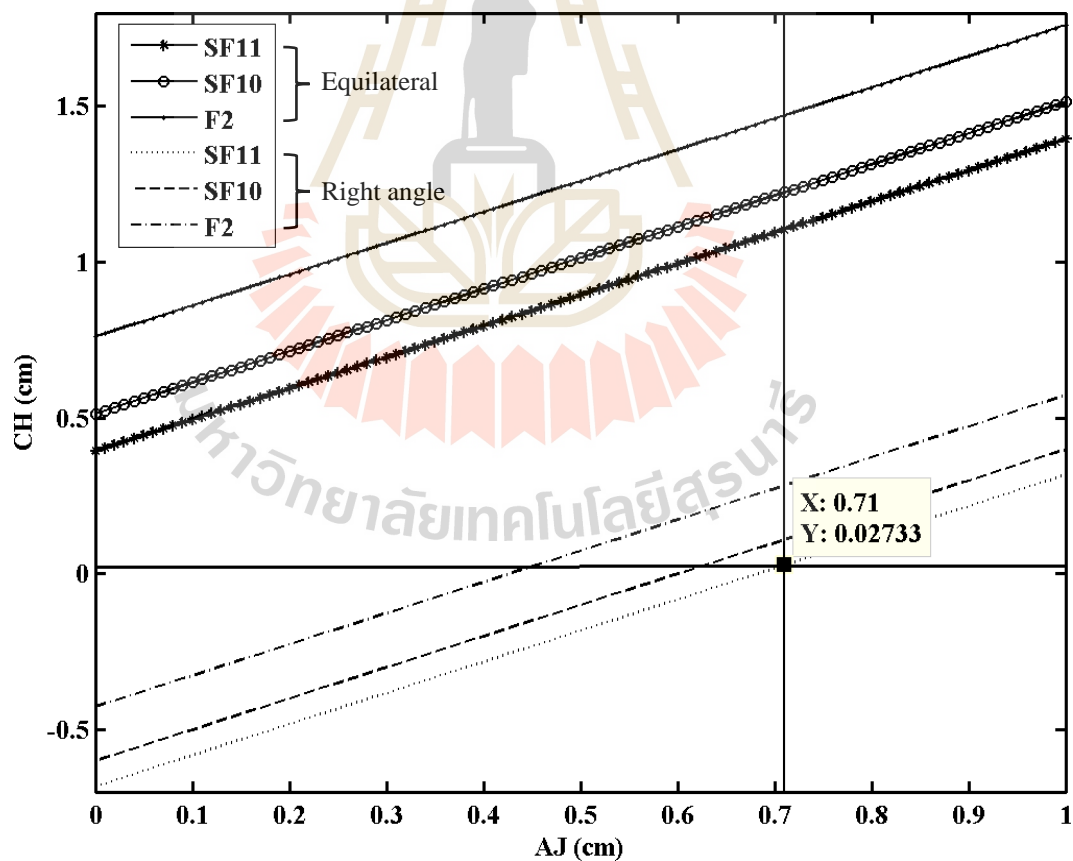
Since, the beam width  $GH$  is dependent upon the beam  $EF$ , the position of the beam  $GH$  is also affected by the distance  $AJ$ . By applying the sine rule to the triangle  $\Delta BFG$ , the beam position  $BG$  is found to be

$$BG = \frac{BF \cos \beta_{i2}}{\cos \beta_{i3}}. \quad (3.7)$$

Substitution Eq. (3.6) into Eq. (3.7) gives

$$BG = \frac{AB \cos \beta_{i2}}{\cos(\beta_{i2} - \alpha)} - AJ - IJ. \quad (3.8)$$

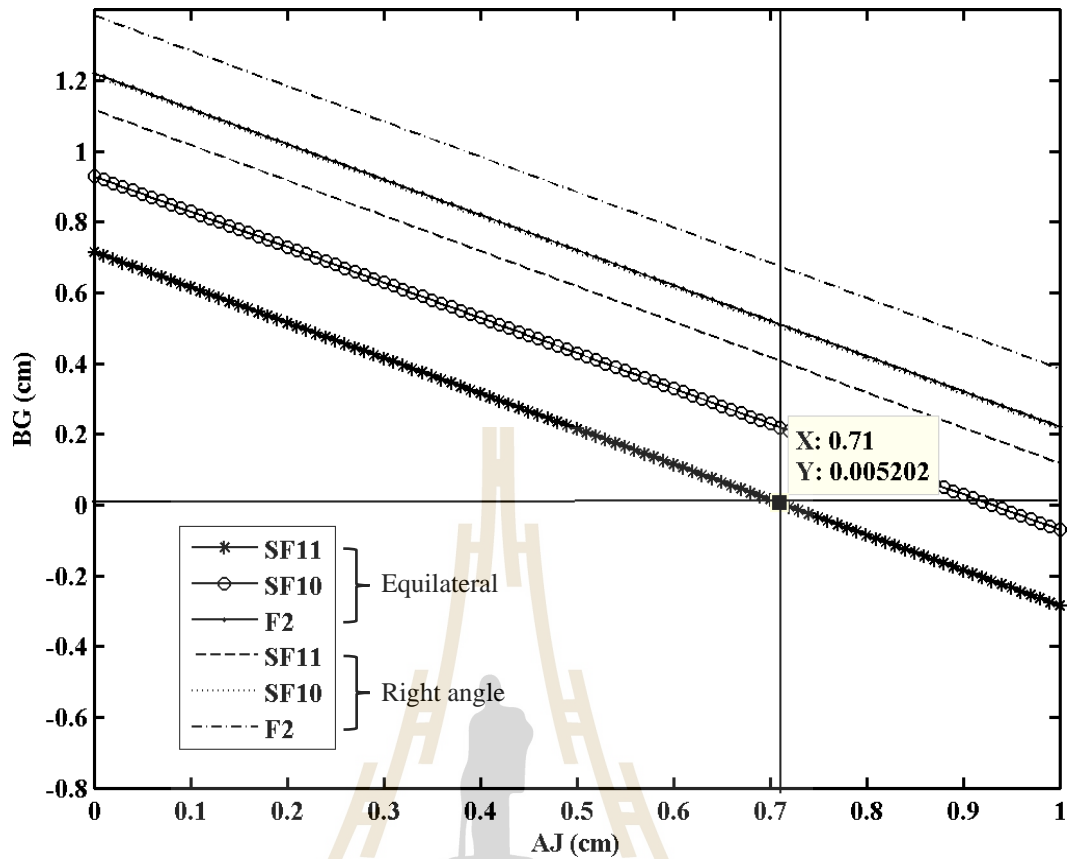
When the value of the distance  $AJ$  increases, the value of the  $BG$  may become zero.



**Figure 3.2** Dependence of  $CH$  on  $AJ$  for the prism side  $AB = 5$  cm.

In order to demonstrate the effect  $AJ$ , the distances  $CH$  and  $BG$  were plotted in Figs. (3.2) and (3.3) by using Eqs. (3.3) and (3.8), respectively. The solid lines with markers represent the equilateral prism, while the dot lines stand for the right angle ones. In Fig. (3.2), the value of  $CH$  of the right angle prism varies from negative to positive as the distance  $AJ$  increases. The negative  $CH$  indicates that the ray  $EH$  is not incident on the surface  $BC$ . This can be explained by considering the argument of arctan in the numerator of Eq. (3.3). For  $AJ = 0$ , this argument reduces to a ratio of  $\cos(\alpha - \theta_2)$  to  $\sin(\alpha - \theta_2)$ . For the right angle prism, the difference between the two angles is smaller than that for the equilateral prism. The cosine of this small angle is nearly unity, however, its sine is very small. Arctan of this very high ratio value gives a resultant angle which is greater than the angle  $2\theta_2$ . As a result, sine of this negative angle difference has negative value. The equilateral prism does not exhibit this tendency, because its apex angle is larger. When the distance  $AJ$  becomes longer, decrease in the ratio results in smaller angle returned by arctan. Furthermore, it is found that the value of  $CH$  is higher for the prism with lower refractive index, because its critical angle is higher.

In Fig. (3.3), the distance  $BG$  varies with negative slope. This can be understood by considering Eq. (3.8) which shows that  $BG$  depends on the value of  $AJ$ . Although the subtraction of the last term from the first term always gives positive value, its value becomes smaller as  $AJ$  increases. The distance  $BG$  is also affected by the prism material through the beam size  $IJ$ . This is because the prism with low refractive index requires smaller incident angles  $\theta_{i1}$  and  $\beta_{i1}$ . Since this causes smaller  $IJ$ , the distance  $BG$  becomes larger. Note that the negative value of  $BG$  represents the situation that ray  $FG$  does not exist.



**Figure 3.3** Dependence of  $BG$  on  $AJ$  for the prism side  $AB = 5$  cm.

Since the two distance  $CH$  and  $BG$  must be positive for both prisms, the distance  $AJ$  is set to be 0.71cm. This result is important for determining the size of the sensing area. This condition in which the ray  $IF$  is incident on the vertex  $B$ , yielding zero ray reflection  $FG$ . Therefore, the beam size  $EF$  given by

$$EF = IJ \frac{\cos(\alpha - \beta_{i2})}{\cos(\beta_{i2})} + AJ \left[ \frac{\cos(\alpha - \beta_{i2})}{\cos(\beta_{i2})} - \frac{\cos(\alpha - \theta_{i2})}{\cos(\theta_{i2})} \right] \quad (3.9)$$

can be derived by applying Snell's law and sine rule to triangles  $\Delta AEJ$  and  $\Delta AIF$ .

Equation (3.9) reveals that the size and the position of  $EF$  depend on the fixed size of



the beam width  $IJ$  and the value of  $AJ$ . Finally, the beam size  $GH$  can be obtained from triangles  $\triangle BEH$  and  $\triangle BFG$  that is

$$GH = AB \left[ \frac{\cos \theta_{i2}}{\cos \theta_{i3}} - \frac{\cos \beta_{i2}}{\cos \beta_{i3}} \right] - AJ \left\{ 1 - \left[ \frac{\cos(\alpha - \theta_{i2}) \cos \beta_{i2}}{\cos \theta_{i2} \cos(\alpha - \beta_{i2})} \right] \right\} + \frac{EF \cos \beta_{i2}}{\cos(\alpha - \beta_{i2})}. \quad (3.10)$$

Equation (3.10) shows that the size of the beam  $GH$  transmitted from the surface  $BC$  highly depends on the length of hypotenuse side of the prism and the beam size  $EF$ . Table 3.3 which shows the beam size  $IJ$ ,  $EF$  and  $GH$  caused by the corresponding fan angles for the right-angle prisms. The beam sizes in the three sides of the prism with higher refractive index are longer than those with lower refractive index. This is because its fan angle is bigger.

**Table 3.3** Beam sizes for different right angle prism material.

Prism RI	$IJ$ (cm)	$EF$ (cm)	$GH$ (cm)
1.785	0.904	2.746	2.873
1.728	0.828	2.561	2.715
1.620	0.6907	2.218	2.404

The same tendency occurs for the case of the equilateral prism shown in Table 3.4. However, since this prism requires bigger fan angle than the right angle, the increase in the fan angle causes bigger beam size.

**Table 3.4** Beam sizes for different equilateral prism material.

Prism RI	<i>IJ</i> (cm)	<i>EF</i> (cm)	<i>GH</i> (cm)
1.785	1.125	3.552	3.608
1.728	0.9529	3.128	3.318
1.620	0.72	2.533	2.838

In order to distribute uniformly the detected beam along the sensor surface, the beam *HL* and *GP* need to have the same angle of the incidence  $\xi$  on the surface. This can be achieved by inclining the sensor to the surface *BC*. The angle  $\xi$  can be found by extending the lines *LH* and *PQ* such that the two lines crosses at an imaginary point. From a reconstructed isosceles triangle, the angle  $\xi$  is found to be

$$\xi = 90^\circ - \frac{1}{2}(\theta_{i3} + \beta_{i3}). \quad (3.11)$$

This angle of incidence corresponds to angle  $\chi$ , which is formed by the sensor and vertical axis. This angle  $\chi$  given by

$$\chi = 90^\circ - \alpha - \frac{1}{2}(\theta_{i3} - \beta_{i3}) \quad (3.12)$$

can be determined by considering  $\Delta B'BG$

Finally, it is important to determine the beam size incident on the detector. This can be done by considering two triangles  $\Delta CHL$  and  $\Delta CGP$ . It is found the incident beam size *LP* is equal to

$$LP = \frac{GH \cos \beta_{i3} \sin \frac{1}{2}(\theta_{i3} + \beta_{i3}) + HM \cos \frac{1}{2}(\theta_{i3} - \beta_{i3})(\cos \beta_{i3} - \cos \theta_{i3})}{\cos \frac{1}{2}(\theta_{i3} + \beta_{i3}) \sin \frac{1}{2}(\theta_{i3} + \beta_{i3})}, \quad (3.13)$$

where  $HM$  is the distance from the prism side  $BC$  to the detector. On other hand, Eq. (3.12) is also useful for finding the position of the detector having known size  $LP$  with respect to prism. The detector position is given by

$$HM = \frac{\sin \frac{1}{2}(\theta_{i3} + \beta_{i3}) \left( LP \cos \frac{1}{2}(\theta_{i3} + \beta_{i3}) - GH \cos \beta_{i3} \right)}{\cos \beta_{i3} - \cos \theta_{i3}}. \quad (3.14)$$



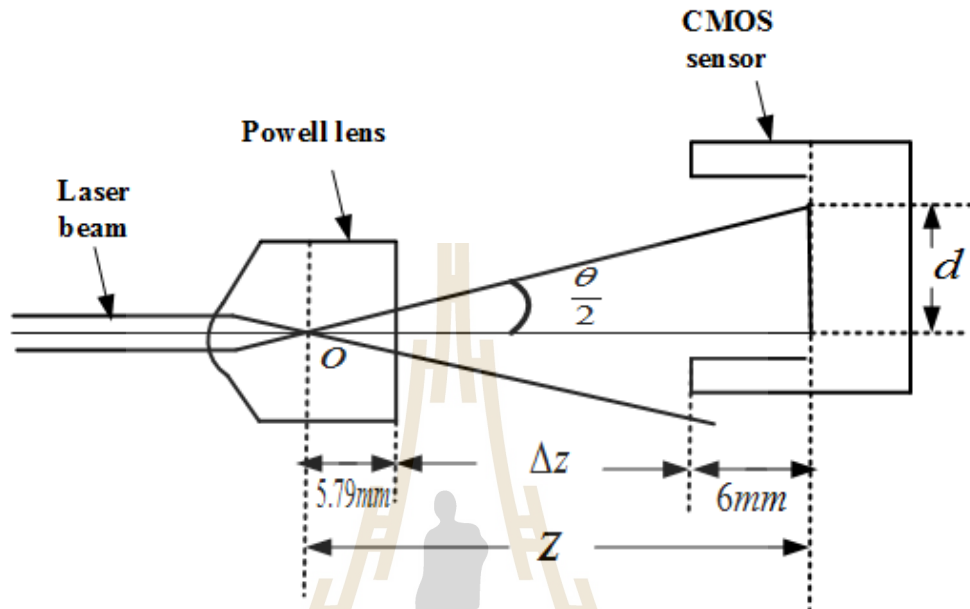
## CHAPTER IV

### EXPERIMENTAL VERIFICATIONS

#### 4.1 Experimental Setup

In order to study feasibility of the proposed SPR sensor, the indices of air and distilled water (4L84X) were measured by using the SPR setup shown in Fig. 3.1. The TM-polarized light was generated from a He-Ne laser (Melles Griot, 05LHP151) with wavelength  $\lambda = 632.8$  nm. Its polarization state was controlled by a combination of a polarizing cube beam splitter (Melles Griot, 03PB007) and a half wave plate (Melles Griot, 02WRQ31/632.8). Powell lens with the fan angle of  $60^\circ$  (Thorlabs, PLO160) diverged uniformly the beam. Due to a smaller fan angle than the required angle in Table 3.2 and the finite size of the sensor chip, the maximum resonance angle  $\beta_{i2max}$  reduced to  $56.62^\circ$ . According to the previous discussion the distance  $AJ$  was set to be equal 7 mm, while  $OI'$  was 8 mm. Its corresponding evanescent wave was generated by 50 mm N-SF11 uncoated equilateral prism (Edmund, #49-432). A gold evaporated glass chip (Nano SPR, BA1000) with size of  $20 \times 20$  mm<sup>2</sup> was placed on top of the prism as the sensor chip with the refractive index matching (Cargille series A). The reflected beam from the sensor chip was detected by using a digital camera (Canon, EOS 60D) with a resolution of  $5184 \times 346$  pixels in an area of  $22.3 \times 14.9$  mm<sup>2</sup> and an imaging lens (Canon, EFS 18 – 55 mm) with a demagnification factor of 1.89.

## 4.2 Measurement of the Fan Angle



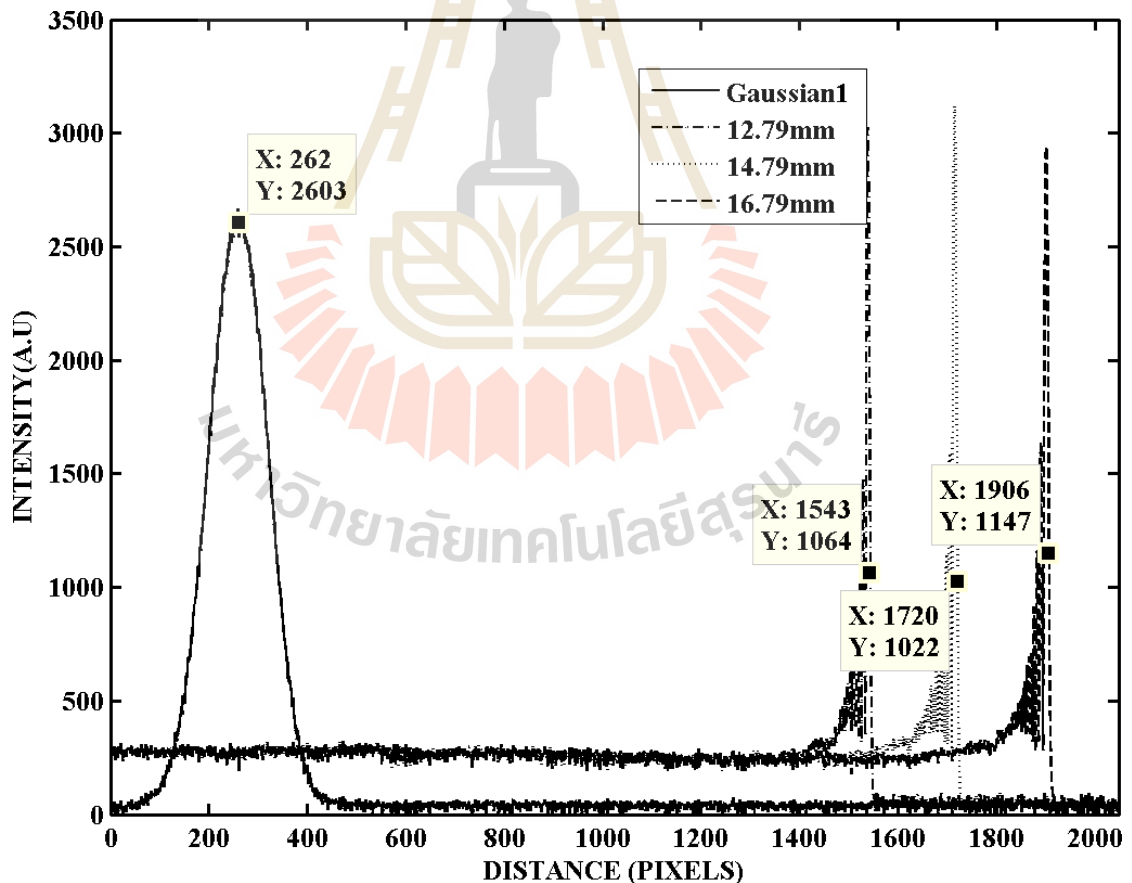
**Figure 4.1** A schematic diagram of an optical setup for measuring the fan angle the Powell lens

In this study, the fan angle of Powell lens was validated by using a setup shown in Fig. 4.1. Since the beam size produced by the lens was bigger than CMOS sensor (Beamage 3.0) which has resolution  $2048 \times 1088$  pixels in the area of  $11.3 \times 6.0 \text{ mm}^2$ , only a half part of the beam  $d$  was measured at three distances  $z$  from 12.79 mm to 17.79 mm with an interval of 2 mm. With known the focusing position inside the lens and the position of the sensor, the half fan angle can be calculated by

$$\tan(\theta/2) = \frac{d}{z} = \frac{n \times \Delta x}{z}, \quad (4.1)$$

where  $n$  and  $\Delta x$  are the pixel number and the pixel size, respectively. Here,  $z$  is given by  $z = 5.79 + \Delta z + 6$ , with  $\Delta z$  is the separation between the lens and the sensor. Figure

4.2 shows beam intensity profiles without and with the Powell lens. Without the lens, the beam had a Gaussian intensity profile. The center of the beam was located at the pixel  $x = 262$ . By installing the Powell lens, the beam size diverged gradually as  $\Delta z$  was increased by moving the sensor away from the lens. It can be observed that the diverging beams recorded at three different distances had uniform intensity distribution, except at their edges. Table 4.1 shows the measured fan angles obtained from the experiment. The errors are still within the divergence angle tolerance is  $\pm 3\%$  specified in its specification.



**Figure 4.2** Diverging beam sizes measured at different positions  $z$ .

**Table 4.1** Fan angles as a function the CMOS sensor position.

$\Delta z$ (mm)	$z$ (mm)	$n$ (pixels)	$d$ (mm)	$\theta/2$ (°)	Fan angle $\theta$ (°)	Error (%)
0	11.79	1281	7.0455	30.9	61.8	3
1	13.79	1458	8.019	30.1	60.2	0.3
2	15.79	1644	9.042	29.8	59.6	-0.7

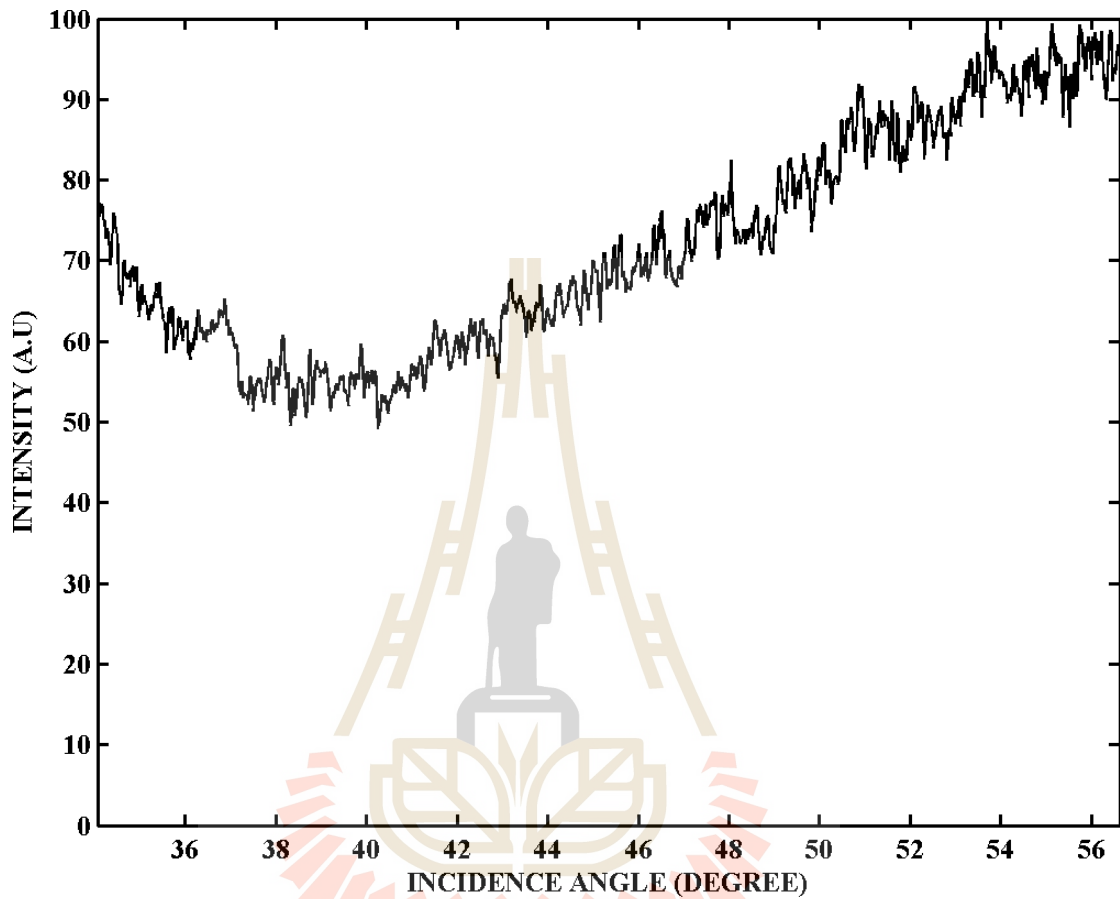
### 4.3 Measurement of Beam Size

In order to verify alignment of the experiment set up, the beam sizes at each surface of the prism were measured by using a millimeter graph paper. Table 4.2 shows a comparison of the theoretical and the measured beam sizes  $IJ$ ,  $EF$  and  $GH$ . Note that the theoretical values were calculated by using the fan angle  $\theta = 60^\circ$  and  $\beta_{i2max} = 64.86^\circ$ . The measured beam sizes are slightly smaller than those of the theory. This may be caused by parallax error on reading scales on millimeter the graph paper and a misalignment of the setup.

**Table 4.2** Beam sizes of SF 11 prism.

Beam size	Theory	Measurement	Error (%)
$IJ$ (cm)	1.125	1.0	11
$EF$ (cm)	3.552	3.3	7.1
$GH$ (cm)	3.608	3.5	3

#### 4.4 Measurement of Refractive Index



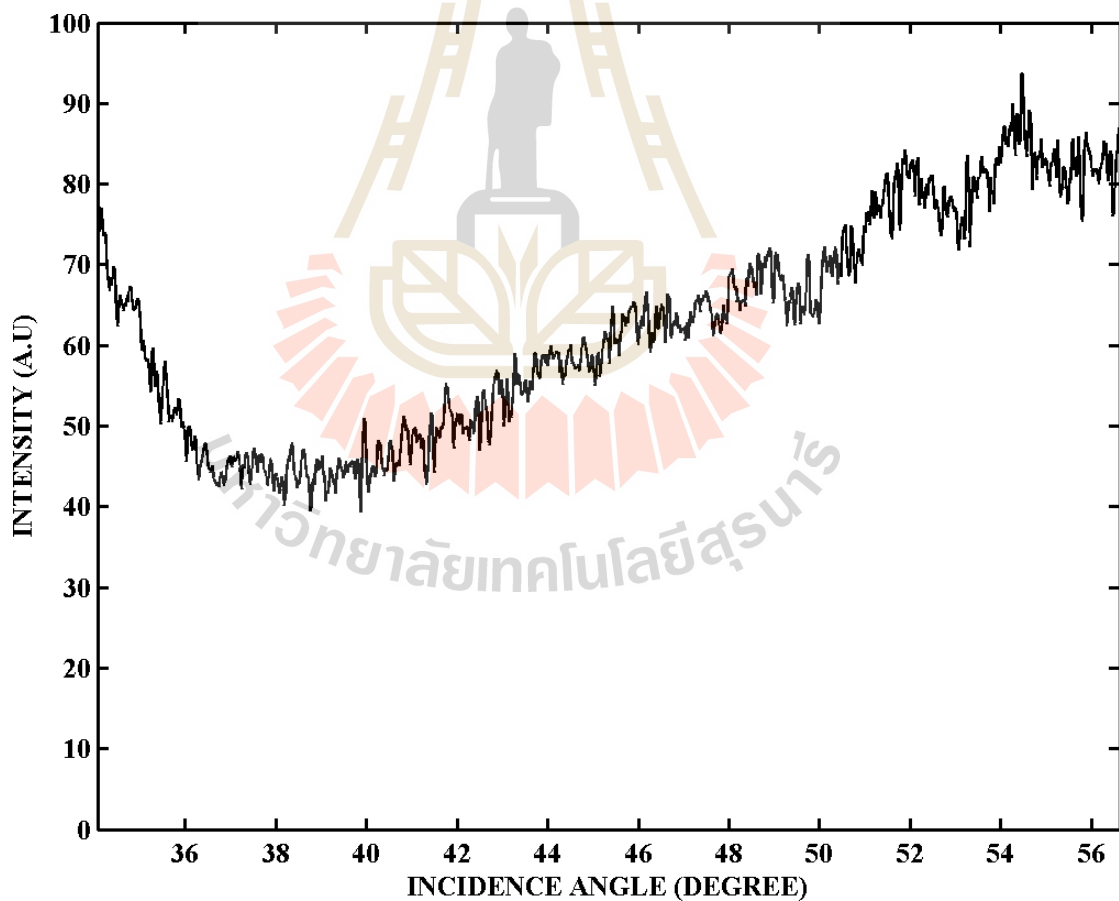
**Figure 4.3** Intensity distribution of the reflected beam *GH* at the screen obtained without using the gold coated glass chip.

Prior the refractive index measurement, the intensity distribution of the reflected beam *GH* produced without the sensor chip was observed by using a tracing paper placed behind the surface *BC* with the distance  $HM = 7$  mm. The beam size at the screen was 5 cm. Figure 4.3 shows the intensity distribution captured by the camera placed behind the screen. In this figure, the intensity at the first pixel



originated from the light reflected at the critical angle of  $34.07^\circ$ , while the last pixel 2014 corresponds to the  $\beta_{sprmax} = 56.62^\circ$ . Therefore, an angular resolution (AR) of this system can be calculated as

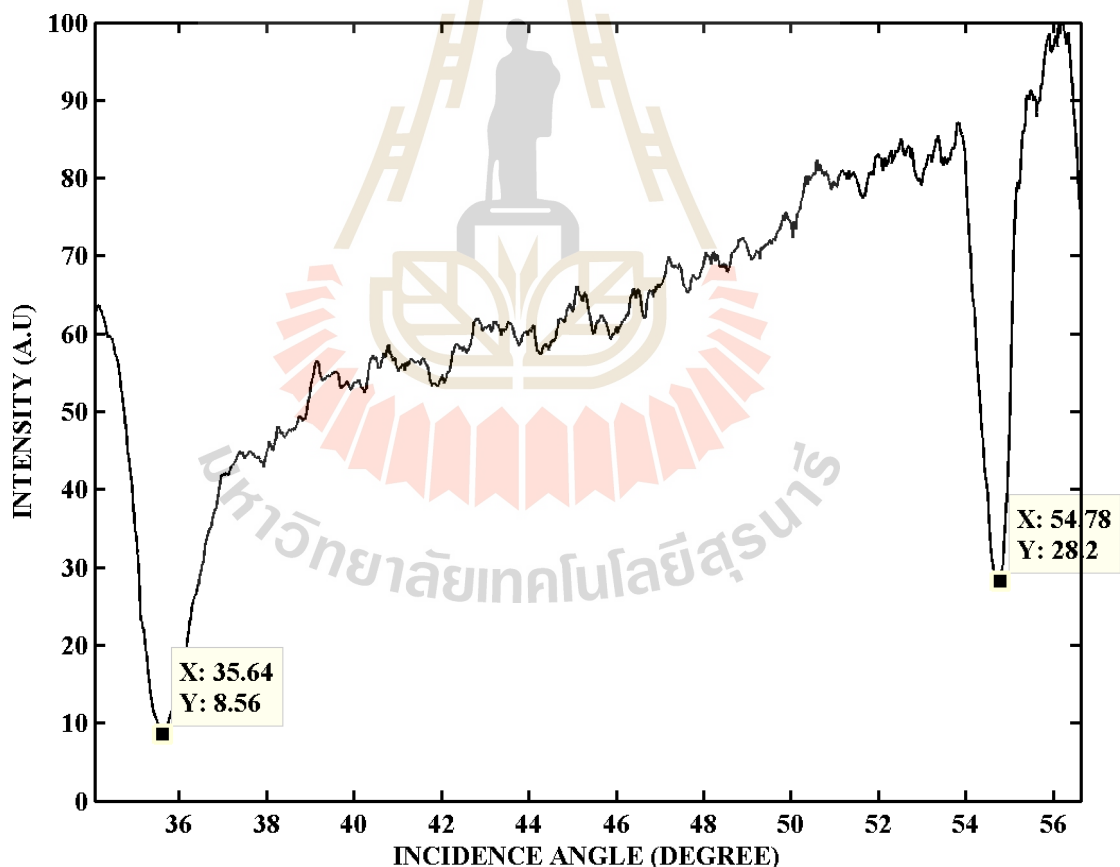
$$\begin{aligned} \text{AR} &= \frac{\text{Range of detected angle}}{\text{Number of pixels}} & (4.2) \\ &= \frac{56.62^\circ - 34.07^\circ}{2014} \\ &= 0.0112^\circ / \text{pixel}. \end{aligned}$$



**Figure 4.4** Intensity distribution of the reflected TE-mode beam *GH*.

The next measurement was done by placing the sensor chip on top of the prism. The TE-polarized beam was used to readout the SPR sensor by rotating the half-wave plate. Figure 4.4 shows the intensity distribution of the reflected beam *GH* obtained by using this configuration. The light has similar intensity distribution as the one shown in Fig. 4.3. This is because no transfer of photon energy from the TE-mode beam onto electrons can occur in the dielectric media.

The last experiment was to measure simultaneously the refractive indices of air and water by using the TM-polarized beam. The captured intensity distribution of



**Figure 4.5** Intensity distribution of the reflected beam with two dip intensities caused by the resonances of air and water.

the reflected beam  $GH$  is shown in Fig. 4.5. It is apparent that there are two occurrences of the dip intensity. The first dip intensity, which appears at the pixel number 140, corresponds to the resonance condition of air. The second one located at the pixel number 1849 is caused by the water. The unbalanced dip intensities may be caused by the contaminated chip. By taking the angular resolution into account, the resonance angle of air from the measurement is found to  $140 \text{ pixel} \times 0.0112^\circ/\text{pixel} + 34.07^\circ = 35.64^\circ$ , while that of water is  $1849 \times 0.0112^\circ/\text{pixel} + 34.07^\circ = 54.78^\circ$ .

As it has been shown by Fig. 2.4 that prism with higher refractive index demonstrates linearity property between resonance angle and changes of the refractive index of the samples thus, the sensitivity of the proposed SPR sensor is defined as (Lan, Liu et al. 2015).

$$\text{sensitivity} = \frac{\beta_{spr-water} - \beta_{spr-air}}{n_{water} - n_{air}} . \quad (4.3)$$

According to Table 3.1 and the resonance angle of air that is 35.86, the theoretical sensitivity calculated by using Eq. (4.3) is equal to 54.98°/RIU. From the experiment, the measured resonance angle can be used to calculate the measured sensitivity. Substitution of the measured angle to Eq. (4.3) gives the measured sensitivity that is equal to 57.82°/RIU. The difference of the sensitivity may be caused by the misalignment of the setup.

## CHAPTER V

### CONCLUSION AND FUTURE WORK

#### 5.1 Conclusion

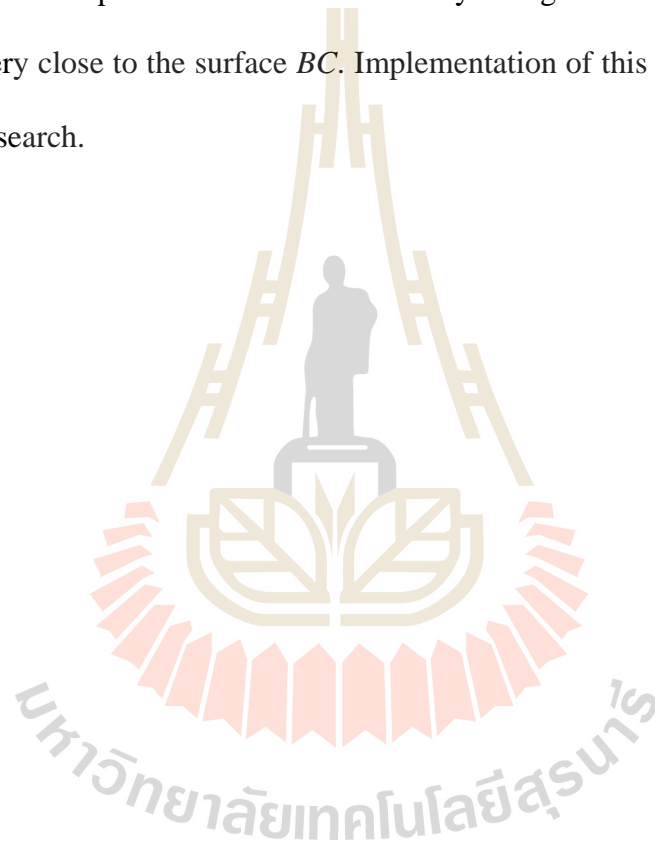
In this thesis, the SPR sensor by using Powell lens has been theoretically studied and experimentally demonstrated. The proposed SPR obviates the mechanical scanning of the resonance angles, because the readout beam produced by the lens is diverging beam. The theoretical studies found that:

- The fan angle of Powell lens depends on the refractive index and the apex angle of the prism such that the higher the refractive index or the bigger the apex angle causes the bigger fan angle requirements.
- Similar dependencies of the beam size on the refractive index and the apex angle of the prism are also found in this study
- In order, not to corrupt the size of the reflected beam  $GH$ , the beam position  $AJ$  needs to be carefully calculated.
- The sensor camera cannot be placed in parallel with the surface  $BC$ , because the detected beam will not be uniformly distributed.

The feasibility of the SPR sensor has been experimentally verified by measuring simultaneously the refractive indices air and water without any mechanical beam scanning. This opens the way to implement easily a multichannel SPR sensor.

## 5.2 Future work

The experimental verification show that the reflected beam diverges rapidly after being transmitted by the surface  $BC$  of the prism. The use of sensor cameras is impractical and bulky, because its sensor is located inside the camera body and the need of the demagnifying lens system. As a result, the angular resolution of the sensor is not high. These problems can be solved by using full frame sensor which is positioned very close to the surface  $BC$ . Implementation of this sensor will be studied for further research.



## REFERENCES

- Bordo, V. G. and H.-G. Rubahn (2008). **Optics and spectroscopy at surfaces and interfaces**, John Wiley & Sons.
- Bouguelia, S., Y. Roupioz, S. Slimani, L. Mondani, M. G. Casabona, C. Durmort, T. Vernet, R. Calemczuk and T. Livache (2013). "On-chip microbial culture for the specific detection of very low levels of bacteria." **Lab on a Chip** 13(20) : 4024-4032.
- Chan, B. L. and S. Jutamulia (2012). "SPR prism sensor using laser line generator." **Proceeding SPIE** (8234):82341P-82341P.
- Dou, X., P.-Y. Chung, P. Jiang and J. Dai (2012). "Surface plasmon resonance-enabled antibacterial digital versatile discs." **Applied Physics Letters** 100(6) 063702.
- Fan, C. and J. Longtin (2000). "Laser-based measurement of temperature or concentration change at liquid surfaces." **Journal of Heat Transfer** 122(4):757 - 762.
- Forzani, E. S., H. Zhang, W. Chen and N. Tao (2005). "Detection of heavy metal ions in drinking water using a high-resolution differential surface plasmon resonance sensor." **Environmental Science & Technology** 39(5): 1257-1262.
- Goodrich, T. T., H. J. Lee and R. M. Corn (2004). "Direct detection of genomic DNA by enzymatically amplified SPR imaging measurements of RNA microarrays." **Journal of the American Chemical Society** 126(13):4086 - 4087.
- Gwon, H. R. and S. H. Lee (2010). "Spectral and angular responses of surface plasmon resonance based on the Kretschmann prism configuration." **Materials Transactions** 51(6): 1150 - 1155.

- Kashif, M., A. A. A. Bakar, N. Arsad and S. Shaari (2014). "Development of phase detection schemes based on surface plasmon resonance using interferometry." **Sensors** 14(9): 15914 -15938.
- Koubova, V., E. Brynda, L. Karasova, J. Škvor, J. Homola, J. Dostalek, P. Tobiška and J. Rošický (2001). "Detection of foodborne pathogens using surface plasmon resonance biosensors." **Sensors and Actuators B: Chemical** 74(1): 100-105.
- Kretschmann, E. and H. Raether (1968). "Notizen: radiative decay of non radiative surface plasmons excited by light." **Zeitschrift für Naturforschung A** 23(12): 2135-2136.
- Lan, G., S. Liu, X. Zhang, Y. Wang and Y. Song (2015). "A simplified high figure-of-merit prism-free surface plasmon resonance refractive index sensor based on self adaptive angular interrogation." **Review of Scientific Instruments** 86(2): 025006.
- Laplatine, L., L. Leroy, R. Calemczuk, D. Baganizi, P. N. Marche, Y. Roupioz and T. Livache (2014). "Spatial resolution in prism-based surface plasmon resonance microscopy." **Optics Express** 22(19): 22771-22785.
- Lavine, B. K., D. J. Westover, L. Oxenford, N. Mirjankar and N. Kaval (2007). "Construction of an inexpensive surface plasmon resonance instrument for use in teaching and research." **Microchemical Journal** 86(2): 147-155.
- Maier, S. A. (2007). **Plasmonics: fundamentals and applications**, Springer Science & Business Media.
- Mouvet, C., R. Harris, C. Maciag, B. Luff, J. Wilkinson, J. Piehler, A. Brecht, G. Gagulitz, R. Abuknesha and G. Ismail (1997). "Determination of simazine in wa-

- ater samples by waveguide surface plasmon resonance.” **Analytica Chimica Acta** 338(1): 109-117.
- Mukhtar, W., P. S. Menon, S. Shaari, M. Malek and A. Abdullah (2013). “Angle shifting in surface plasmon resonance: experimental and theoretical verification.” **Journal of Physics: Conference Series**, (431) IOP Publishing. 012028.
- Nikitin, P., A. Beloglazov, V. Kochergin, M. Valeiko and T. Ksenevich (1999). “Surface plasmon resonance interferometry for biological and chemical sensing.” **Sensors and Actuators B: Chemical** 54(1): 43-50.
- Palumbo, M., C. Pearson, J. Nagel and M. Petty (2003). “A single chip multi-channel surface plasmon resonance imaging system.” **Sensors and Actuators B: Chemical** 90(1): 264-270.
- Pluchery, O., R. Vayron and K.-M. Van (2011). “Laboratory experiments for exploring the surface plasmon resonance.” **European Journal of Physics** 32(2): 585.
- Powell, I. (2004). “Linear diverging lens.” **US Patents**. 4,826,299.
- Otto, A. (1968). “Excitation of nonradiative surface plasma waves in silver by the method of frustrated total reflection.” **Zeitschrift für Physik** 216(4): 398-410.
- Raether, H. (1988). “**Surface plasmons on smooth surfaces.**” Springer.
- Schasfoort, R. B. M. and A. McWhirter (2008). “Chapter 3 SPR Instrumentation.” **Handbook of Surface Plasmon Resonance**, The Royal Society of chemistry: 35-80.
- Schermer, M. (2007). “Plasmon resonance measuring method and apparatus,” **US Patents**. 7,271,885.
- Tao, N., S. Boussaad and W. Huang (2004). “Surface plasmon resonance detection with high angular resolution and fast response time,” **US Patents** 6,784,999.



- Taylor, A. D., J. Ladd, Q. Yu, S. Chen, J. Homola and S. Jiang (2006). “Quantitative and simultaneous detection of four foodborne bacterial pathogens with a multi-channel SPR sensor.” **Biosensors and Bioelectronics** 22(5): 752-758.
- Tobiška, P., O. Hugon, A. Trouillet and H. Gagnaire (2001). “An integrated optic hydrogen sensor based on SPR on palladium.” **Sensors and Actuators B: Chemical** 74(1–3): 168-172.
- Yanase, Y., T. Hiragun, S. Kaneko, H. J. Gould, M. W. Greaves and M. Hide (2010). “Detection of refractive index changes in individual living cells by means of surface plasmon resonance imaging.” **Biosensors and Bioelectronics** 26(2): 674-681.
- Yap, W. F., M. Yunus, W. Mahmood, A. Moxsin, M. Maarof, Z. A. Talib and N. A. Yusof (2011). “Surface plasmon resonance optical sensor for mercury ion detection by crosslinked chitosan thin film.” **Journal of Optoelectronics and Advanced Materials** 13(3): 279-285.

## **BIOGRAPHY**

Mr. Jordan Hakim Hossea was born on 26 August 1986 in Kilombero District at Morogoro region, Tanzania. He earned his Bachelor degree in Electronic and communication Engineering from St. Joseph university in Tanzania in 2012.

He then worked as tutorial assistant at St Joseph University October 2012 – October 2013. After that, I moved to Dar es salaam Institute of Technology where I worked as tutorial assistant January 2014 – July 2015.

He then continued his Master's Degree in the school of Electronic Engineering, Institute of Engineering, Suranaree University of Technology, Nakhon Ratchasima, Thailand (July 2015- July,2017). His fields of interest include optical sensors and instrumentation, bioelectronic and bioelectromagnetic sensor. While he was pursuing his Master's degree study, he presented one international paper entitled; "Design of surface plasmon resonance biosensors by using Powell lens" in the 5th International Electrical Engineering Congress, 8 – 10 March 2017 in Thailand.